Viticulture extension in response to global climate change drivers - lessons from the past and future projections

Joel Guiot[1], Nicolas Bernigaud[1], Alberte Bondeau[2], Laurent Bouby[3], Wolfgang Cramer[2]

[1]Aix-Marseille Université, CNRS, IRD, INRAE, CEREGE, Aix-en-Provence, France
[2] Institut Méditerranéen de Biodiversité et d'Écologie marine et continentale (IMBE), Aix Marseille Université, CNRS, IRD, Avignon Université, Aix-en-Provence, France
[3] ISEM, Université Montpellier, CNRS, IRD, EPHE, Montpellier, France

Correspondence to: Joel Guiot (guiot@cerege.fr)

Abstract.

The potential areal extent of agricultural crops is sensitive to climate change and its underlying drivers. To distinguish between the drivers of past variations in the Mediterranean viticulture extension since Early Antiquity and improve projections for the future, we propose an original attribution method based on an emulation of offline coupled climate and ecosystem models. The emulator connects the potential productivity of grapevines to global climate drivers, notably orbital parameters, solar and volcanic activities, demography and greenhouse gas concentrations. This approach is particularly useful to replace the evolution of future agrosystems in the context of their past variations. We found that variations in potential area for viticulture during the last three millennia in the Mediterranean Basin were mainly due to volcanic activity, while the effect of solar activity and orbital changes were negligible. In the future, as expected, the dominating factor is the increase in greenhouse gases, causing significantly drier conditions and thus major difficulties for viticulture in Spain and North Africa. These constraints will concern significant areas of the Southern Mediterranean Basin when global warming exceeds +2°C above pre-industrial conditions. Our experiments showed that even an intense volcanic activity comparable to that of the Samalas - sometimes considered as the starting point of the Little Ice Age at the mid 13th century - would not decrease aridity and so not slow down this decline in viticulture extension in the southern margin of the Mediterranean area. This result does not confirm the idea of geoengineering that solar radiation modification (SRM) is an efficient option to limit the future global warming.

Keywords climate model emulator, Mediterranean area, viticulture, Holocene, future scenarios, forcing attribution

1 Introduction

Our scientific question is related to the attribution the viticulture extension changes - which has an economical role in the Mediterranean Basin since Antiquity - to any natural or anthropogenic drivers. The cultivation and domestication of the

30 grapevine began between the 7th and 4th millennia before the common era (BCE) between the Eastern Mediterranean and Caspian areas, and spread to Egypt, the Middle East and the entire Mediterranean (Terral et al., 2010; Bouby et al., 2021). Introduced in the Gaul region (i.e. roughly France and surrounding regions) by Greek colonists ca. 600 BCE, around the time they settled Marseilles, viticulture was initially limited to Mediterranean Gaul (Bouby et al., 2014). Vineyards expanded into the northern part of Gaul in the 1st century CE, where wine production developed quite considerably in the following centuries

35 up to the Paris region, and the Rhine and Moselle valleys (Brun, 2010), and even in southern England (Brown et al., 2001). One hypothesis behind this expansion is the climate warming during the Roman Climatic Optimum (RCO) (Mccormick et al., 2012). These climate variations are driven by global forcing variables such as solar or volcanic (Wanner et al., 2008; Brayshaw et al., 2010; Fuks et al., 2017). After the RCO, the temperature decreased significantly and Gaul entered the so-called Late Antique Little Ice Age, or LALIA (536-660 CE) (Büntgen et al., 2016). This change may have been triggered by to several

40 large volcanic eruptions at 536, 540 and 547 CE (Sigl et al., 2015). This assumption remains difficult to prove because of the limited historical and archaeological sources. In any case, the 500 to 900 CE period remained relatively cold with oscillating precipitation changes in the region (Reale and Dirmeyer, 2000). In Europe, the following Medieval Climate Anomaly (MCA, approx. 900-1200 CE) (Luterbacher et al., 2016) was likely of comparable intensity to the RCO. The Little Ice Age (LIA, approx. 1250-1850 CE) was a period of alpine glacier advance (Holzhauser et al., 2005), marked again by several large volcanic

45 eruptions, in particular that of the Samalas (Indonesia) in 1257 (Lavigne et al., 2013).

On timescales of centuries and millennia, quality and yield of agricultural crops are strongly affected by climate fluctuations. The nature of the change depends on external forcings and internal feedbacks of the climate system, which produce different spatial and seasonal patterns of the main variables in the atmospheric environment. The main objective of this paper is to develop an innovative solution to statistically model the impact of changing climate forcing on vegetation over several

50 millennia, using the grapevine (a major crop of the Mediterranean and European region) as example. We mimic this impact model on the basis of a large ensemble of existing model simulations, using statistical relationships much faster to be computed (Kennedy and O'Hagan, 2000). Based on a large range of climate states from high-resolution simulations with coupled earth system models for the last glacial period to future global warming scenarios, this approach called emulator provides robust results and can be applied to a large range of ecosystem processes under different conditions.

55 The global drivers of the studied changes are anthropogenic - greenhouse gases emissions (GHG), land use and cover changes, population density, economic production - and natural – earth orbit, volcanic and solar activity. They are the boundary conditions of Earth System Models (ESM) (Kay et al., 2014). The ecosystem processes are assessed using impact models (IM) coupled to these ESMs (Franklin et al., 2016; Warszawski et al., 2014; Frieler et al., 2017). In most cases, coupling is offline because (i) the spatial scales of ecosystems are much finer than are those of earth system, thus making it necessary a scale

60 transfer (Su et al., 2016); (ii) a climate simulation of a given ESM is interpreted as one realization out of a set of possibilities determined by the boundary conditions and the characteristics of the ESM, thus making necessary to work on ensembles of models to be representative of the climate system (Kay et al., 2014); and (iii) each ESM has intrinsic biases that must be corrected before it can be used to drive the ecosystem model (Williamson et al., 2015).

2

Even if human innovation and colonization were also responsible for the expansion of viticulture, the climate must be suitable for grape cultivation and thus remains a control variable. As soon as the climate changes to worse conditions for wine growth, it becomes a driver of a decline in viticulture. Such fluctuations are particularly noticeable near the Northern range limit of wine growth during the end of the Roman and Medieval periods with a regression of the grape cultivation.

Although we focus our viticultural analysis on the Gaul region (France and surrounding countries), we need to enlarge the area to the entire Mediterranean and European surrounding region to robustly capture the relationships between global drivers and viticulture extension. For the same reason, we use a large diversity of time slices of the past (Last Glacial Maximum, Mid-Holocene, last millennium) and of the future up to 2100 according to several scenarios. The widely diverse situations used for calibration made it possible to produce a robust emulator that was effective for extrapolating a wide range of past and future climate states. This method is particular appropriate to establish a bridge between past variations of a given agrosystem to its future evolution. Once calibrated, the emulator is of great help to efficiently support decision in the domain of impacts of climatic change.

2 Material and method

As ESMs are an imperfect representation of reality, our approach has the same limitations even if the model parameters are carefully chosen (Crucifix, 2012). The same author develops the idea that the Bayesian framework is adequate to stimulate the modelling of the distance between the ESM and reality. So the ESM's produce a certain vision of the world that needs to converge to the reality represented by the paleodata. This procedure is called data assimilation which provides a way to reduce the uncertainties.

The concept of our method and the data used are presented in Fig.1. Global forcings are the inputs of low-resolution ESMs. Step 1 involves adapting output fields to a common high-resolution grid using statistical downscaling. This step is also useful to correct the systematic biases of the ESM simulations. Step 2 involves applying the vegetation model BIOME4 to the high-resolution fields to calculate ecosystem variables. Steps 1 and 2 are repeated for each ESM simulations available. These simulations based on different forcings and different models provide a large and diversified calibration dataset. They are a guarantee that the emulator is in some way more robust than the ESM simulations taken separately. Calibration of the emulator (step 3) is done by spatial regression of the ecosystem variables on the forcing variables. Step 4 involves the application of the emulator to the forcings of new time slices or future scenarios. During this step, the annual temperature and precipitation results for the past time slice were compared to paleodata to identify the amplitude of the volcanic and solar activity effects (data assimilation). Step 5 is the independent validation of the emulator using tree-ring data.

Figure 1. Diagram of the different steps in the emulator approach; the ecosystem variables, related to bioclimate and net primary productivity, are defined in Table 1. Low density hashes in the trapezes indicate low resolution of the corresponding data and high density hashes correspond to higher resolution.

3
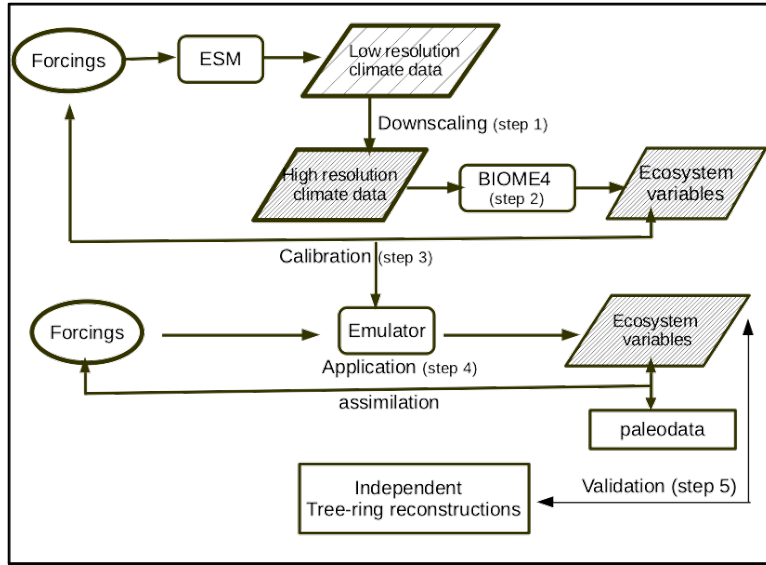
Table 1. The biome types simulated by BIOME4 and output variables used for the paper; note that there is no correspondence between the two columns.

N°	Biome names	Ouput variables
1	Tropical evergreen forest	NPPtot : total net primary production
2	Tropical semi-deciduous forest	Dominant PFT (plant function type)
3	Tropical deciduous forest/woodland	AET actual evapotranspiration (mm)
4	Temperate deciduous forest	MTCO mean temperature of the coldest month (°C)
5	Temperate conifer forest	MTWA mean temperature of the warmest month (°C)
6	Warm mixed forest	E/PE actual over potential evapotranspiration
7	Cool mixed forest	GDD5 growing degree-days above 5°C (° days)
8	Cool conifer forest	TANN annual mean temperature (°C)
9	Cold mixed forest	PANN annual sum of precipitation (mm)
10	Evegreen taiga/montane forest	
11	Deciduous taiga/montane forest	
12	Tropical savanna	NPP net primary production of following PFTs
13	Tropical xerophytic shrubland	Tet: Tropical Evergreen Trees
14	Temperate xerophytic shrubland	Trt: Tropical Drought-deciduous Trees (raingreens)
15	Temperate sclerophyll woodland	Tbe: Temperate Broadleaved Evergreen Trees
16	Temperate broadleaved savanna	Tst: Temperate Deciduous Trees
17	Open conifer woodland	Ctc: Cool Conifer Trees
18	Cool Desert	Bec: Boreal Evergreen Trees
19	Tropical grassland	Bst: Boreal Deciduous Trees
20	Temperate grassland	tg: C3/C4 temperate grass plant type
21	Hot Desert	Trg4: C4 tropical grass plant type

22	Steppe tundra	Wds: C3/C4 woody desert plant type
23	Shrub tundra	Tsg: Tundra shrub type
24	Dwarf shrub tundra	Ch: cold herbaceous type
25	Prostrate shrub tundra	Lf: Lichen/forb type
26	Cushion forb lichen moss tundra	
27	Barren	
28	Land ice	

2.1 The forcing variables

115 Climate forcing or drivers are perturbations imposed on the Earth's energy balance. They are mainly:

(i) Orbital parameters: eccentricity (*ecc*) and obliquity of the ecliptic (*obl*), solar longitude at the perihelion (*omega*); they drive the orbit of the Earth and influences the climate of the Earth by modulating the solar energy intercepted by the planet and its seasonal distribution at time scales above thousands of years (Berger and Loutre, 1991); they had a major impact on the Earth climate from the last glacial period to the Holocene; at the century time-scale, the orbital parameters do not operate

120 significantly, so the values of the last millennium can be linearly interpolated between the values at 1000 yr BP and the present values, and the values of the 21st century can be set to the present values.

(ii) Greenhouse gas concentration (GHG): carbon dioxide (CO_2), methane (CH_4) and nitrous oxide (N_2O); the effect of these GHG has been significant from the glacial to interglacial periods and has a major effect for the current century (see for example Fig.2 for CO_2).

125 (iii) The world population values taken from the Hyde 3.1 database for the past periods from (Klein Goldewijk et al., 2011) and for the future periods from (van Vuuren et al., 2011). The population varied from less than 10^6 at the LGM to $7 \cdot 10^9$ in 2010 and is projected to be between $9 \cdot 10^9$ and $12.3 \cdot 10^9$ in 2100 according to the scenario.

(iv) Volcano activity (V) represented by the effective aerosol radius deduced from the aerosol optical depth from ice core sulfate records from both polar regions for the last millennium (Crowley and Unterman, 2013) (Fig. 2). Its value is 0.2 when

130 there is no eruption. The maximum value (0.8) was found in 1258, the year after the Samalas eruption (Lavigne et al., 2013). The 21ka, 6ka and future values were set to the pre-industrial values.

(v) Solar activity (S) is inferred from ^{14}C records, the proxy of the total solar irradiance (TSI) (Muscheler et al., 2007) for the last millennium, and varies from 0 to 1200 MeV (Fig. 2). The 21ka, 6ka and future values were set to the pre-industrial values.

135 Figure 2. Natural (volcanic activity and solar activity) and anthropogenic forcing (CO_2) for the last millennium. Upper panel: the effective aerosol radius which is directly related to the aerosol optical depth is calculated by Crowley and Unterman (2013) ; middle panel: the proxy indicating the total solar irradiance (TSI), i.e. the solar modulation function in MeV based on ^{14}C (Muscheler et al, 2007); lower panel: atmospheric CO_2 concentration (in ppm). The horizontal red lines represent the mean values of the five selected periods.
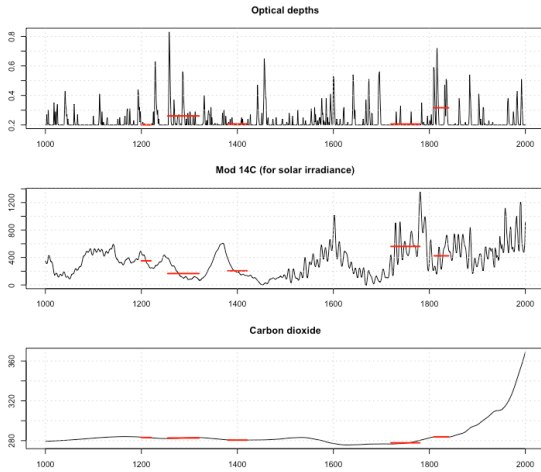
Optical depths

Mod 14C (for solar irradiance)

Carbon dioxide

150 **2.2 The past time climate data (used for calibration)**

The past time periods retained for calibration are (1) the Last Glacial Maximum (21ka) characterized by very low greenhouse gases (GHG), large *ecc, obl* (close to present value) and very negative *omega* orbital parameters; (2) the mid Holocene (6 ka) characterized by GHG close to pre-industrial period, relatively large *ecc*, large *obl* and slightly negative *omega*; (3) five periods of the last millennium (Fig. 2) representing various combinations of S and V forcings: V-S+ (1200-1220), V+S- (1255-1320),

155 V-S+ (1380-1420), V-S++ (1720-1780), V+S+ (1810-1840); (4) the pre-industrial (PI) reference period with intermediate GHG concentrations, low *ecc,* large *obl*, large *omega*, large V and S.

The simulations were archived by the Paleoclimate Modelling Intercomparison Project (PMIP), which produced snapshot simulations of the mid-Holocene (6 ka BP) and Last Glacial Maximum (21 ka BP) time slices to study the effects of insolation, greenhouse gases and massive ice sheets on the climate, https://pmip3.lsce.ipsl.fr/overview/ (Braconnot et al., 2012). The

160 models used for intercomparisons were coupled atmosphere-ocean-vegetation models with various levels of complexity and resolution (Table 2).

Table 2. CMIP5 and PMIP3 simulations used in the paper. First column is the code of model, the second the institute which built the model; the other columns provide the availability of the scenarios or time slices. Hist. = historical period (last millennium), MidHol = Mid Holocene

165 (6 kyr BP), LGM = Last Glacial Maximum (21kyr BP).

Model	Institute	RCP 2.6	RCP 4.5	RCP 8.5	Hist.	Mid Hol	LGM

6

bcc-csm1-1	Beijing Climate Center, China Meteorological Administration	X	X	X		X	
bcc-csm1-1-m	Beijing Climate Center, China Meteorological Administration	X	X	X			
CCSM4	Community Climate System Model Contributors, UCAR-NSF-DoE-NASA, USA					X	X
CCSM4b	Community Climate System Model Contributors, UCAR-NSF-DoE-NASA, USA					X	X
CanESM2	Canadian Centre for Climate modelling, Canada	X	X	X			
CESM1-BGC	Community Earth System Model Contributors, NSF-DoE-NCAR, USA		X				
CSIRO-Mk3	CSIRO Marine and Atmospheric Research, Victoria, Australia					X	
CSIRO-Mk3L	CSIRO Marine and Atmospheric Research, Victoria, Australia				X	X	
CMCC-CM	Centro Euro-Med per Cambiamenti Climatici, Italy		X	X			
CNRM-CM5	Centre National de Recherches Météorologiques / Centre Européen de Recherche et Formation Avancée en Calcul Scientifique, France	X	X	X		X	X
COSMOS-ASO							X
FGOALS-g2	LASG, Institute of Atmospheric Physics, Chinese Academy of Sciences and CESS,Tsinghua University, China					X	
FGOALS-s2	LASG, Institute of Atmospheric Physics, Chinese Academy of Sciences and CESS,Tsinghua University, China					X	X
GFDL-CM3	NOAA Geophysical Fluid Dynamics Laboratory, USA	X	X				
GISS-E2-H	NASA Goddard Institute for Space Studies, USA	X	X	X			
GISS-E2-H-CC	NASA Goddard Institute for Space Studies, USA						
GISS-E2-R	NASA Goddard Institute for Space Studies, USA	X	X	X		X	X
GISS-E2-Rb	NASA Goddard Institute for Space Studies, USA						X
HadCM3	Met-Office – Hadley Center, UK				X		
HadGEM2-AO	Met-Office – Hadley Center, UK	X	X	X			
HadGEM2-ES	Met-Office – Hadley Center, contributed by Instituto Nacional de Pesquisas Espaciais, Spain	X					
inmcm4	Inst. For Numerical Mathematics, Russia		X	X			
IPSL-CM5A-LR	Institut Pierre-Simon Laplace, France	X	X	X		X	X
IPSL-CM5A-MR	Institut Pierre-Simon Laplace, France	X	X	X			
IPSL-CM5B-LR	Institut Pierre-Simon Laplace, France						
MIROC-ESM	University of Tokyo, National Institute for Environmental Studies, and Japan Agency for Marine-Earth Science and Technology					X	X
MPI-ESM-LR	Max-Planck Inst. für Meteorologie, Germany	X	X	X			
MPI-ESM-P	Max-Planck Inst. für Meteorologie, Germany					X	X
MPI-ESM-MR	Max-Planck Inst. für Meteorologie, Germany	X	X	X			
MRI-CGCM3	Meteorological Research Institute, Japan	X	X	X		X	X
NorESM1-M	Norwegian Climate Centre	X	X	X			
NorESM1-ME	Norwegian Climate Centre	X	X	X			
Nb simulations		16	18	16	2	13	11

2.3 The future climate data (used for calibration)

170 The future periods are determined by increasingly high GHG concentrations (depending on the scenario, see below), and the other forcing variables were set to the PI value. The simulations were archived by the Coupled Model Intercomparison Project (CMIP). We used simulations of CMIP5 (Taylor et al., 2012). These include both (i) century-scale integrations, which usually start from a preindustrial control, and climate predictions until the end of the 21st century, and (ii) near-term integrations for the next 10 to 30 years, which are initialized using observed ocean and sea-ice conditions. The CMIP5 climate change

175 projections are driven by emission scenarios, divided into four classes referred to as "representative concentration pathways" (RCPs) (Moss et al., 2010). The high-emissions scenario, named RCP8.5 or "business as usual", refers to a high radiative forcing of emissions at the end of the 21st century (8.5 W m^{-2}). The low-emission scenario, which roughly represents that of the Paris Agreement, reaches its maximum value near the middle of the century before decreasing to a level of 2.6 W m^{-2} at the end of the century. We only used the intermediate scenario RCP4.5 which refers to a radiative forcing maintained at values

180 of 4.5 W m^{-2} at the end of the 21st century. We used 10 time slices interpolated at a 10-year steps (2010, 2020, …, 2100). The forcing variables for the future scenarios were obtained from the website http://www.iiasa.ac.at/web-apps/tnt/RcpDb.

2.4 The application data

We used our emulator to analyze the response of key ecosystem variables to global forcing. We focused on past periods that were marked by important climate and societal changes (Table 3). The present time slice was defined by the mean values for

185 the 1961-1990 period. For the future, instead of using time slices, we defined the scenarios according to the global temperature signal simulated in the different models, using the relationship between global warming and CO_2 concentration (Guiot and Cramer, 2016):

(i) The +1.5°C global warming recommended by the Paris Agreement is reached with a CO_2 concentration of 440 ppm; Fig.3 shows that the average model simulation reaches this value under scenario RCP2.6 in approximately 2040.

190 (ii) The +2°C global warming is reached with a CO_2 concentration of 480 ppm and is reached under scenario RCP4.5 in approximately 2050 (Fig.3).

(iii) The +3°C global warming is reached with a CO_2 concentration of 600 ppm and is reached under scenario RCP8.5 in approximately 2060 (Fig.3).

(iv) The +5°C global warming is reached with a CO_2 concentration of 900 ppm and is reached under scenario RCP8.5 in about

195 2090 (Fig.3);

We obtained the corresponding CH_4 and N_2O concentrations and population sizes from the boundary condition database of CMIP5. The other future forcings are set to the present values.

Following Giorgi and Lionello (2008), the study area was divided into nine grid boxes (Fig. 4). We added a 10th box corresponding to the Gallia Narbonensis Roman province (south of France), the key area for the introduction of viticulture in

200 Gaul.

We also considered two other scenarios, based on boundary conditions of +5°C except for volcanic and solar activity. The idea is to assess whether volcanic and solar conditions typical of the Little Ice Age can moderate the effect of the strong increase

205 in GHG concentrations. The first additional scenario (labeled +5CV+) was assigned very substantial volcanic activity (0.8), the highest value in the last millennium, and low solar activity (i.e. 100). In contrast, the second additional scenario (labeled +5CV-) was assigned low volcanic activity (0.1) and high solar activity (700), corresponding to those of the MCA. The forcing values are listed in Table 2.

210 Table 3. Typical past periods used to calibrate our emulator. The paleoclimatic and societal information are found in the literature given in the references, from the Late Holocene to the Present.

Time slices and labels	Location	Climate	Societal events	References
4200 (4200-3900 yr BP)	Levant, Mesopotamia, Sicily	Drought	Collapse of Akkadian empire in Mesopotamia	(Kaniewski et al., 2018; Weiss and Bradley, 2001; Magny et al., 2013)
3200 (3300-2900 yr BP)	The Levant, Anatolia, Aegean, Egypt Mesopotamia	Drought	Collapse/decline of Aegean, Hittite, Palestinian, Egyptian, Babylonian civilizations	(Roberts et al., 2011; Kaniewski et al., 2015) (Neumann and Parpola, 1987)
2500 (2600-2400 yr BP)	West Med, France Maghreb	Cold Dry	Early Iron Age	(Finné et al., 2011; Magny et al., 2013) (Leveau, 2009)
2000 (2100-1800 yr BP)	West Med, France, Maghreb	Warm, wet	Roman Climate Optimum (RCO), expansion of the empire	(Mccormick et al., 2012; Büntgen et al., 2016)
1300 (1410-1290 yr BP or 536-660AD)	West Med, Alps Mesopotamia, Iran	Cold Dry	Late Antique Little Ice Age (LALIA) (migrations, pandemics, social turmoil) Demise of Sasanians	(Büntgen et al., 2016) (Sharifi et al., 2015)
1000 (1150-650 yr BP or 800-1300AD)	Europe, Alps, East	Warm dry	Medieval climate anomaly (MCA)	(Telelis, 2008)(Büntgen et al., 2011), (Izdebski et al., 2016; Finné et al., 2011)
700 (700-600 yr BP or 1250-1350 AD)	Europe, Alps	Cold	Beginning of Little Ice Age (LIA); famine, black death	(Büntgen et al., 2011; Luterbacher et al., 2016)
200 (300-230 yr BP or 1650-1720)	Europe, Alps Spain	Cold wet Dry	Max of Little Ice Age (LIA); famines	(Magny et al., 2013; Büntgen et al., 2011) (Magny et al., 2013)
Present (1961-1990)	All areas	Warm and dry		CRU data (Jones et al, 2012)

Figure 3. Global annual temperature anomalies (T) simulated by the various models of PMIP3 and CMIP5, according to the
215 reference period average (1961-1990). The left graphic represents the past simulations, the right graphic represents the present and future projections for three scenarios (RCP2.6 in green, RCP4.5 in orange, RCP8.5 in red). Each dot represents one model simulation. The vertical scales are shifted for a better readability. The reference is given by the New et al (2002) dataset calculated on the 1961-1990 period. The anomalies versus the pre-industrial period are obtained by adding approximately 0.5°C the 1961-1990 anomalies.
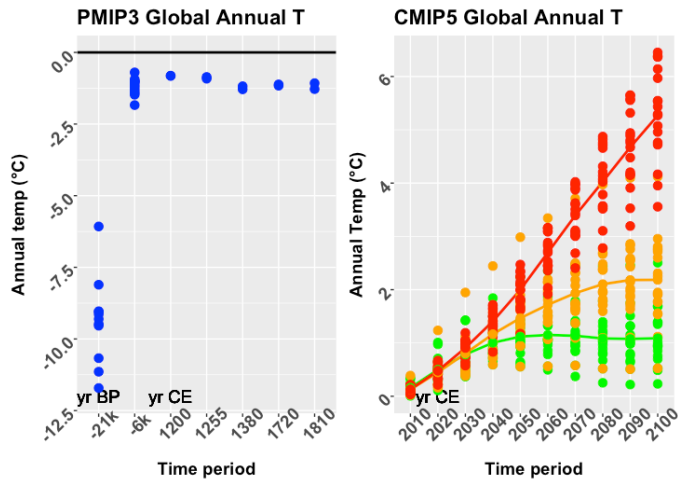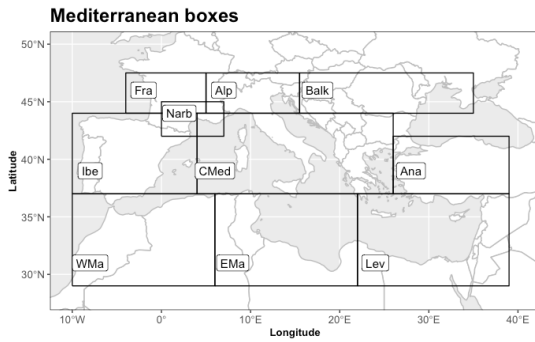220

Figure 4. Map of the 10 boxes defined in the Mediterranean region.

235

2.5 Downscaling (step 1)

ESM resolution is too coarse (>100 km depending on the model) to assess the impact and risk of climate changes on ecosystems or human systems. Different approaches can be used to derive higher-resolution information. We use a statistical downscaling (SD), based on statistical relationships that link large-scale atmospheric variables with local/regional climate variables and that are applied to coarser-resolution model simulations (Su et al., 2016; Grouillet et al., 2016; Levavasseur et al., 2011), so providing higher-resolution estimates of climate variables. SD methods are among the less computably expensive downscaling techniques.

The SD that we use assumes the hypothesis that the fields of climate anomalies do not depend on the grid resolution. So, they can be interpolated at a finer resolution than the initial resolution. We use a common 0.5° high-resolution (HR) grid for each climate simulation. It is provided by the high-resolution data set of surface climate over global land areas (New et al., 2002) (which has a 10 minutes resolution and was aggregated at a 30 minutes resolution). This climatology is based on the 1961-1990 period. Each low-resolution (LR) anomaly field provided by the ESM is downscaled to the HR grid by the bilinear interpolator of platform R (function *interp.surface* of package *fields*). This HR anomaly field is added to the 1961-1990 climatological HR field of New et al (2002). As the simulations are corrected by the differences between control simulations and observations, the main systematic biases of the model are removed. For the PMIP3 simulations (LGM, MidHol and historical), the control is the pre-industrial simulation (PI) so we use the 1900-1931 climatology very close to the PI (1861-1890) used by the recent IPCC reports (Allen et al., 2018). Fig.3 presents the global mean temperature for each period and scenario considered.

2.6 Vegetation modeling (BIOME4, step 2)

The ecosystem model is coupled offline to downscaled climate outputs and provide indications on land vegetation structure and productivity. Here, we used a process-based equilibrium vegetation model, BIOME4 (Kaplan et al., 2002), which has been successfully applied to similar questions before (Guiot and Cramer, 2016). While a wide range of climate simulations are necessary to ensure robust calibration, the use of a single ecosystem model is required to ensure that the same ecosystem variables are calculated for all simulations.

BIOME4 simulates some of the most important processes related to vegetation at the scale of the ecosystem, specifically photosynthesis, respiration, evapotranspiration. It predicts structure and productivity of broad-scale land ecosystems from monthly temperature and rainfall values and annual CO_2 concentration. It uses a photosynthesis scheme that simulates acclimation of plants to changed atmospheric CO_2 by optimization of nitrogen allocation to foliage and by accounting for the effects of CO_2 on net assimilation, stomatal conductance, leaf area index (LAI) and ecosystem water balance. BIOME4 is based on sufficiently simple description of ecophysiological processes to allow broad-scale application. It represents substantial advantages over niche-models because it has not been tuned to reproduce present-day potential vegetation, but

11

rather to simulate correctly the main processes underlying the potential vegetation distribution which are assumed to have been similar throughout the Holocene. BIOME4 does not account for human land use.

270 The inputs of the model are monthly average values of temperature, precipitation and sunshine percentage, atmospheric CO_2 concentration, and soil texture. The temperature and precipitation variables are directly obtained from the simulations downscaled at the 0.5° grid. The sunshine percentages are obtained by linear regression on temperature and precipitation (Guiot et al., 2000). The absolute minimum temperature is derived from the mean temperature of the coldest month according to the quadratic equation of Prentice *et al* 1992. The soil data are provided by the FAO (Zobler, 1986). The CO_2 atmospheric

275 concentration values are those considered by CMIP5 and PMIP3 as boundary conditions for their simulations.

The outputs include net primary production (NPP) of each of the potentially occurring 13 plant functional types (PFT), the total NPP and the corresponding 'biome type', from a set of 28 broad categories (Table S1). The model provides also several bioclimatic variables presented also in Table 1.

2.7 The calibration of the emulator (step 3)

280 The numerous model outputs available in the CMIP and PMIP databases (Table 2) are used to calibrate robust statistical approximations of coupled ESMs and BIOME4, called emulator (Kennedy and O'Hagan, 2000). Various emulators are used in climate science (Tran et al., 2016; Zhu et al., 2015; Rougier and Goldstein, 2014; Castruccio et al., 2014), including in paleoclimatology (Strassmann and Joos, 2018; Joos et al., 1996; Bounceur et al., 2015). Our approach is the first ESM-independent emulator because it is calibrated using a large set of model simulations under very different scenarios. The

285 calibration is based on a geographically weighted regression (Brunsdon et al., 1998), where the ecosystem variables are expressed as functions of the global forcing variables.

For any choice of input q-vector $\boldsymbol{x}$ (forcings), the climate simulator $y(\boldsymbol{x}, s) = (y_1(\boldsymbol{x}, s), \dots, y_m(\boldsymbol{x}, s))$, where m is the number of (bio)climatic variables whose response is to be analysed and s is the location where the climate variables must be estimated. There are deterministic and possibly non-linear functions. This model is a statistical representation of the ESM+BIOME4

290 model, with the very interesting properties to run very fast and provide an uncertainty description for the whole plausible input space (i.e. conform to physics, internally consistent and reasonable (Amara, 1991)).

$$y_j(\boldsymbol{x}, s) = X \beta_j(s) + e_j(s) \quad j = 1, \cdots, m; s = 1, \dots, n \qquad (1)$$

where s indicates the grid point out of a total of n points, $y_j(\boldsymbol{x}, s)$ is the anomaly of the climatic variable j (out of m) at location s, i.e. the climate variable at time t minus the climate variable at time 0 (present), X is a matrix with v specified columns of the

295 input global forcings (they do not depend on the location s), and $e(s)$ is a stationary gaussian variable $N(0, \sigma_j^2)$. This can be considered as a least-square problem where the coefficients $\beta_j(s)$ are estimated to minimize the sum of the squared errors. These coefficients can be written as

$$\hat{\beta}_j(s) = (X^T W(s) X)^{-1} X^T W(s) y_j \qquad (2)$$

with W(s) is a matrix of weights specific to location s such that observations nearer to s are given greater weight than observations further away, T is the transpose symbol. The estimation of $\beta_j(s)$ in location s is provided by weighting all the observations according to their distance from s, d_{is}. The method is called "Geographically Weighted Regression" (GWR) (Brunsdon et al., 1998). We use a bisquare weighting function, so that W(s) is the diagonal matrix with elements

$$w_{is} = (1 - \left(\frac{d_{is}}{h}\right)^2)^2 \;\; if \; d_{is} < h \;\; and \;\; 0 \;\; if \; d_{is} > h \tag{3}$$

h is called the bandwidth. We use here the function *gwr.basic* of package *gw.model* on R (Lu et al., 2014). We have chosen h=8 (in longitude and latitude degree units).

The emulator is trained on an ensemble of simulations performed on data browsing sufficiently well the plausible input space. The more the input space is filled, the more robust the emulator will be. The fact that we have extended the range of forcing parameters to past, present and future scenarios is an excellent way to fill this input space. Even if they are not an fully exhaustive sampling, it is reasonable to assume that they represent a model population (Chandler, 2013). The emulator is used to estimate the conditional probability distribution of the ecosystem variables (Table 1) in each location or biome, based on the forcing variables (Table 4).

Table 4. The nine global forcing variables and their values for the different periods considered. The global forcing variables are the predictors of the emulator; we give their values for the time slices used in the calibration: GHG atmospheric concentration (carbon dioxide, methane, nitrogen protoxide) in ppm, earth orbit parameters (eccentricity Ecc, obliquity Obl, omega Ω), population in million people (M), volcanic activity (Volc), solar activity (Sol, in MeV). Every column is one out of the v forcings of eq. 1 (columns of X). For columns CO_2, CH_4, N_2O and Population, we use observations until 2010 (see section 2.1) and the values used by the three scenarios (RCP2.6, RCP4.5, RCP8.5) for projections (2020 to 2100).

Time period	CO$_2$	CH$_4$	N$_2$O	Ecc	Obl	Ω	Population	Volc	Sol
21k	185	350	200	0.0196	23.4	-213	2M	0.3	270
6k	280	650	270	0.0190	24.2	-27	28M	0.3	270
1200	280	650	270	0.0170	23.6	85	394M	0.2	400
1255	280	650	270	0.0170	23.6	85	396M	0.4	200
1380	280	650	270	0.0170	23.6	85	390M	0.2	200
1720	280	650	270	0.0170	23.6	85	768M	0.2	600
1810	280	650	270	0.0167	23.4	102	1082M	0.5	400
2006	379	1754	319	0.0167	23.4	102	6542M	0.3	270
2010	389	1773	323	0.0167	23.4	102	6958M	0.3	270
2020	412,412,416	1731,1801,1824	329,330,332	0.0167	23.4	102	7510M, 7505M, 7530M	0.3	270
2030	431,435,449	1600,1830,2132	334,337,342	0.0167	23.4	102	8200M, 8180M, 8800M	0.3	270
2040	440,461,489	1527,1842,2399	339,344,354	0.0167	23.4	102	8800M, 8500M, 9400M	0.3	270
2050	443,487,541	1452,1833,2740	342,351,367	0.0167	23.4	102	9000M, 8900M, 10400M	0.3	270
2060	442,509,604	1365,1801,3076	343,356,381	0.0167	23.4	102	9100M, 9000M,10700M	0.3	270
2070	437,524,677	1311,1745,3322	344,361,394	0.0167	23.4	102	9150M, 9050M, 11500M	0.3	270
2080	432,531,758	1285,1672,3490	344,365,408	0.0167	23.4	102	9150M, 9050M, 11900M	0.3	270

13

2090	426,534,845	1268,1614,3639	344,369,421	0.0167	23.4	102	9150M, 8950M, 12050M	0.3	270
2100	421,538,936	1254,1576,3751	344,372,435	0.0167	23.4	102	9050M, 8800M, 12300M	0.3	270

The total number of simulations available for 18 time slices and three scenarios (for the 2020 to 2100 time slices) from 2 to 18 models is 582. As each one simulates climate for 65,559 grid points of the globe (after downscaling), the total of available observations is ~4 10^7. Because of their strong spatial correlation, it is not necessary to use all the grid points. To have a balance between the different biomes represented on the Earth, for each time slice and each model, we randomly draw a subset of grid points in each biome proportional to its representativity (the proportion of gridpoints with that biome). So, the calibration is done on about 3 10^5 observations (the number is slightly lower than expected because some biomes are absent in some simulations).

As the global forcing variables have the same value for all the grid points for a given time slice and scenario, this may produce problem for the computation of the emulator; we have then added to them a small noise value (a gaussian value with mean=0 and standard deviation equal to the initial standard deviation divided by 100).

Because of collinearity between the predictors (the global forcing variables), their dimensionality is reduced using principal components (PC) of the normalized variables. The nine variables are reduced into five PC explaining together 89% of their total variance. The first PC is mainly related to the greenhouse gases and the global population which is strongly correlated with them. PC3 shows the opposition between solar and volcanic activity. The other ones are difficult to be interpreted.

The 13 PFTs are aggregated into eight PFTs, representing the main types of vegetation across the world (Table 5). This enables to reduce the dimension of ecosystem variables vector. The number of variables to be estimated by the emulator is finally reduced to 17 (predictands in Table 6).

For comparison, we first apply a simple linear model to the data. Table 6 shows that most of the bioclimatic variables are not well fitted. Indeed, only 9 on 17 have a proportion of reconstructed variance higher than 10% (column R2(lm)), which shows well that a single linear model is not adapted to our objective. The gwr is much better as the half of the bioclimatic variables have a squared-R higher than 0.50, but at the cost of a much larger effective number of parameters (ENP) (ENP ~1311 vs 6 for the global linear model). As we have a very high number of observations (~3 10^5), the gwr regressions remain very significant. This is illustrated in Fig.5 by the maps of the regression coefficients spatial distribution (they are standardized by their standard error which comes to the t-value). The degree of smoothing is defined by the bandwidth h (here set to 8). With a lower h, the patterns should be much patchier and the ENP should become much larger, so diminishing the prediction capability of the model.

The interpretation is not straightforward because the predictors are not the forcing parameters but their PCs. Nevertheless, a partial interpretation is possible by using the correlation of the PCs with the forcings. For example, PC1 is correlated with the greenhouse gases (GHG) and the population size, Fig.5 (Tann/PC1) shows that the maximum impact of the GHG on temperature is on Russia. Fig.5 (Pann/PC1) shows that the GHG have a negative effect on the precipitation around

a supprimé: 8

Mediterranean and northern Africa and a positive effect on Russia. The decrease of precipitation according to the increase of
355 GHG is a well-known feature in the Mediterranean (Giorgi and Lionello, 2008). Fig.5 shows also that the annual temperature
(Tann / Pred vs Obs) is well emulated with a strong correlation with CO_2. It is also true, but in a lesser measure, for NPPtot.
The annual precipitation estimates have a much lower variance than the observations.

Table 5. Aggregation of the plant functional types (PFT). The 13 original PFT are defined in Table 1.

aggregated PFT (aPFT)	original PFT (PFT)
Tropical trees (trt)	tet, trt
Temperate Broadleaved Evergreen Trees (tbe)	tbe
Temperate trees (tet)	tst, ctc
Boreal trees (bot)	bec, bst
C3/C4 temperate grass plant type (teg)	tg
C4 tropical grass plant type (trg4)	trg4
C3/C4 woody desert plant type (wds)	wds
Tundra grass/shrub (tug)	tsg, ch, lf

360

Table 6. The t-values of the linear regression between the PFT and bioclimatic variables and the five PCs of the forcing variables with the squared R of the linear model and the gwr-model. For the latter, the coefficients cannot be displayed in a table and are represented as maps in Fig. 5.

| Predictands	Intercept	PC1	PC2	PC3	PC4	PC5	R2(lm)	R2(gwr)
NPPtot	132	194	-53	45	-20	-7	0.36	0.59
trt	61	98	-25	24	-11	-13	0.13	0.78
tbe	37	42	-15	14	-7	-5	0.03	0.25
tet	106	145	-44	39	-21	-15	0.25	0.61
bot	-27	-3	18	-14	8	0	0.01	0.29
teg	110	154	-36	32	-17	-16	0.26	0.74
trg4	52	77	-22	23	-15	-25	0.09	0.52
wds	290	380	-146	120	-61	2	0.71	0.88
tug	-19	-31	5	-9	7	19	0.02	0.19
AET	23	48	9	5	-5	-55	0.07	0.28
MTCO	121	310	-28	58	-43	-99	0.59	0.76
MTWA	299	387	-100	104	-65	-107	0.71	0.77
E/PE	20	4	-4	11	-11	-22	0.01	0.16
P-E	28	-4	-19	13	-8	8	0.01	0.17
GDD5	309	488	-88	109	-71	-110	0.78	0.87
TANN	279	486	-66	97	-67	-138	0.78	0.88
PANN	36	39	-5	14	-10	-42	0.05	0.28

365

Figure 5. Local (longitude x latitude) response of a few (bio)climatic variables to the PCs of forcing variables. The colors represent the t-values (t-val) of the response (= regression coefficient / standard error). Maps 1 to 5 represent the first five PCs;

15

Map 6, the square-R of the regressions; Maps 7 and 8 represent the estimates for low CO_2 (<290 ppm, LGM and Mid-Holocene) and high CO2 (>600 ppm, second half of 21st century with scenario RCP8.5) respectively. The last graphic represents the estimates in function of the observations: blue dots are for observations with CO2<250 ppm, green dots for CO2 belonging to [250, 400] ppm, orange dots for [400, 600] ppm, red dots for CO2>600 ppm. The first series of maps are for the net primary production of the ecosystem (NPPtot), the second for annual temperature (Tann), the last one for annual precipitation (Pann).
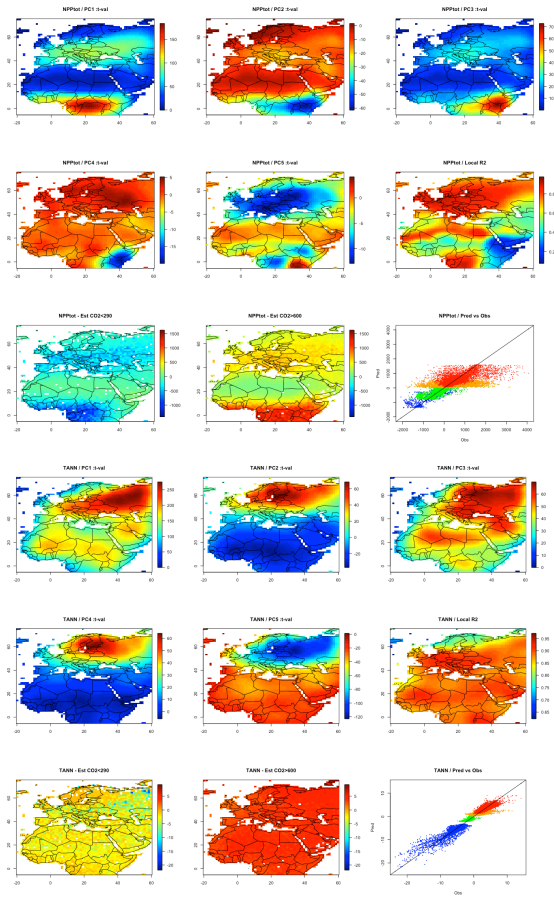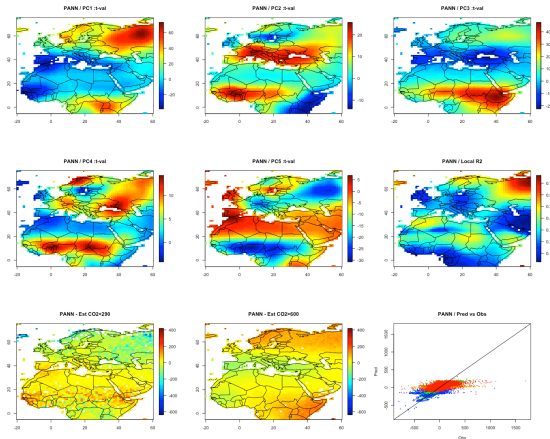
380

2.8 Paleodata assimilation (step 4)

The climatic data estimated by the emulator have biases and uncertainties likely larger than those of the ESM's which have generated the calibration data. The first source of errors of the emulator is the same than the source of errors of the ESM's
385   which are imperfect representations of the real world. The second source of errors comes from the oversimplication which consists in replacing a complex model by a statistical model, in particular in considering that a few global forcings are able to generate the complex observed climate field. It is partly compensated by the fact that the emulator is based on a large diversity of model simulations, at the contrary of a single ESM. The third source of errors is due to the variance of the error terms $e_j(s)$ of eq. (1): the statistical model does not perfectly fit the data. This prompted us to converge the emulator estimates to the real
390   world represented by the paleoclimate data. This is known as paleodata assimilation (Goosse et al., 2012). This lead to adjust a few parameters, known having a large uncertainty, to optimize temperature and precipitation using information given by proxies (Table 7).

These uncertain parameters are: (i) local impact of volcanic activity, (ii) local impact of solar activity, (iii) a possible global
bias for the temperature simulation (δT) and (iv) for the precipitation simulation (δP), (v) the standard error of temperature
395   (σT) and (vi) of precipitation (σP). Parameters (iii) and (iv) are related to a possible global ESM bias and are then independent of the geographical position. Parameters (v) and (vi) express the mean quadratic difference between observations and simulations and then contains the ESM mean error and the emulator mean error (after removing the effects of biases δT or δP).

a supprimé: that may be optimized using temperature and precipitation data,…

17

400 The reconstructed annual temperature and precipitation values are expressed as anomalies relative to the present day for each time slice and each box given in Table 7. It shows that the first two time slices (4200 and 3200 yr BP) were characterized by dry conditions in the eastern Mediterranean Basin (boxes Lev, Ana). All the other time slices are characterized by temperature changes.

The statistical simplification of the emulator makes it possible to run it thousands of times in a relatively short computational
405 time as required by the assimilation methods (Widmann et al., 2010). We use a Bayesian approach called the Markov Chain Monte Carlo method (MCMC), which makes it possible to converge towards the best parameters in the sense of probability distribution (Hargreaves and Annan, 2002).

Starting from the *prior* probability distributions of the six parameters, available climate reconstructions and model outputs provide estimates of their posterior probability distributions. For each time period, these six parameters were optimized to
410 provide the best *posterior* probability distribution of mean temperature and precipitation at the centres of the ten Mediterranean boxes. The *prior* probability distributions are given by uniform distributions delimited by the ±d (Table 8) for the volcanic and solar activity. The *prior* distribution of the other parameters was assumed to be uniform within wide ranges so that they were considered as non-informative for the purpose of this study.

From information given in Tables 3 and 7, we consider that the 4200 and 3200 yr BP time slices provide robust paleoclimatic
415 information for precipitation, and that the other periods provide robust information for temperature. Both the precipitation and temperature signals were robust for the present time slice. Even if we ultimately calculate both temperature and precipitation, only the robust variable(s) is (are) used to constrain the emulator.

420 Table 7. Proxy-based reconstruction of annual temperature (TANN, °C) and annual precipitation (PANN, mm). The values are expressed as anomalies from the pre-industrial period for the 10 spatial boxes and the 9 time slices, obtained from pollen (Guiot and Kaniewski, 2015) and corrected/precised as indicated in Table 3 of the main text.

TANN	WMa	EMa	Lev	Ana	CMed	Ibe	Fra	Alp	Balk	Narb
4200 BP	0.14	0.14	0.02	-0.48	-0.26	0.26	0.62	0.26	-0.6	0.62
3200 BP	-0.08	-0.08	-0.15	-0.04	-0.08	-0.02	0.16	0.05	-0.2	0.16
2500 BP	0.24	0.24	0.13	-0.12	-0.2	-0.13	-1.22	-1	-1	-1.22
2000 BP	0.04	0.04	0.18	0.18	0.5	0.5	0.8	0.5	-0.02	0.5
1300 BP	0.03	0.03	-0.14	0.09	-0.25	-0.2	-0.43	-0.43	-0.68	-0.43
1000 BP	-0.07	-0.07	-0.17	-0.07	0.07	0.09	0.54	0.41	-0.25	0.54
700 BP	-0.07	-0.07	-0.25	0.27	0.09	-0.5	-0.8	-0.8	0.25	-0.8
200 BP	-0.3	-0.3	-0.33	-0.15	-0.3	-0.3	-0.5	-0.5	-0.5	-0.5
Present	1.4	1.3	1.2	1.4	1.4	1	1.2	1.5	1.5	1.2

PANN	WMa	EMa	Lev	Ana	CMed	Ibe	Fra	Alp	Balk	Narb
4200 BP	48.4	48.4	-80	-88.7	29.94	40.83	18.11	51.92	42.84	18.11
3200 BP	-6.84	-6.84	-33	-50.04	4.11	5.13	41.03	34.74	2.82	41.03
2500 BP	61.33	61.33	-34.03	-14.8	25.58	43.78	-8.9	35.35	3.02	-8.9
2000 BP	-11.18	-11.18	4.23	10.3	34.61	-2.78	22.4	47.35	10.2	22.4
1300 BP	20.41	20.41	-11.98	-5.78	67.64	27.34	48.13	94.55	36.31	48.13
1000 BP	-8.72	-8.72	-24.36	-26.77	40.28	-0.45	24.36	51	39.21	24.36
700 BP	37.51	37.51	-37.45	-7.43	1.94	25.73	-9.59	16.18	-29.73	-9.59
200 BP	68.77	68.77	-37.65	-3.47	-2.94	63.72	48.56	21.99	-12.64	48.56
Present	-40	-20	-20	0	-40	-40	-50	0	0	-20

Table 8. Forcing variables used for the 15 time slices/scenarios. The forcing greenhouse gas atmospheric concentrations (CO_2, CH_4, N_2O), orbital parameters (ecc: eccentricity, Obl: obliquity, Omega), population size (POP) in number of people, volcanic activity with uncertainty (d), solar activity with uncertainty (d).

Period	CO2	CH4	N2O	Ecc	Obl	Omega	POP	Volc [delta]	Sol [delta]
4200	280	650	270	0.0181	23.9	34	64138	0.2 [0.2]	200 [200]
3200	280	650	270	0.0178	23.8	45	101664	0.2 [0.2]	200 [200]
2500	280	650	270	0.0175	23.75	65	146283	0.6 [0.2]	270 [200]
2000	280	650	270	0.0175	23.7	68	188239	0.2 [0.2]	400 [300]
1300	280	650	270	0.0174	23.65	75	218535	0.6 [0.2]	270 [200]
1000	280	650	270	0.0173	23.65	75	295040	0.2 [0.2]	400 [300]
700	280	650	270	0.0175	23.5	90	396811	0.6 [0.2]	270 [200]
200	280	650	270	0.0169	23.4	95	813664	0.6 [0.2]	270 [200]
Present	400	1730	330	0.0167	23.45	102	7500000	0.2 [0.2]	600 [300]
+1.5C	440	1527	339	0.0167	23.45	102	8200000	0.2 [0.2]	270 [200]
+2C	487	1833	350	0.0167	23.45	102	8200000	0.2 [0.2]	270 [200]
+3C	603	3076	381	0.0167	23.45	102	8200000	0.2 [0.2]	270 [200]
+5C	900	3700	430	0.0167	23.45	102	12300000	0.2 [0.2]	270 [200]
5CV+	900	3700	430	0.0167	23.45	102	12300000	0.8 [0.2]	100 [200]
5CV-	900	3700	430	0.0167	23.45	102	12300000	0.1 [0.2]	700 [200]

2.9 The viticulture index VI

We subsequently applied our emulator to the question of how viticulture has evolved in the Mediterranean region and in response to which climatic stimuli and global forcing. Numerous bioclimate indices have been published to delimit viticultural zones in the world (Tonietto and Carbonneau, 2004; Santos et al., 2012; Howell, 2001). Among them cite (1) the sum of degree-days above 10°C during the growing season or the heliothermal index of Huglin (HI), (2) the number of days with a minimum temperature below -17°C which is very important for the grapes growing in continental climates, (3) the minimum temperature of September (cool night index CI) important for the ripening, (4) the sum on the growing season of the monthly temperature multiplied by monthly precipitation (Hyl), and (5) the drought stress index (DI) related to the potential water balance of the soil during the growing season. Malheiro et al. (2010) have proposed a composite index (CompI) calculated based on the ratio of years simultaneously satisfying four criteria (HI>1400 degree-days, DI>-100 mm, Hyl<5100 °C*mm and Tmin >-17°C).

Some of the climate variables needed for these indices were not available from the BIOME4 outputs. However, other variables, such as those associated with the net primary production of plant types are very interesting because they include the CO_2 effect on photosynthesis and water use efficiency. Considering only rainfed viticulture, we propose the following index VI:

$$VI = (1 - I_{NPPtrop}) \cdot I_{NPP} \cdot I_{Pann} \cdot I_{MTWA} \cdot I_{MTCO} \cdot I_\alpha \qquad (4)$$

Where each of these factors denoted I_x follows this function:

$$I_x = 0 \; for \; x < x_{min}$$
$$I_x = 1 \; for \; x > x_{max}$$
$$I_x = \frac{x - xmin}{(xmax - xmin)} \; for \; x_{min} \leq x \leq x_{max}$$

for x=NPP$_{trop}$, the net primary production of tropical plants, interval [x_{min}, x_{max}] is [0, 10 kg C m^{-2}];

for x=NPP, the total ecosystem net primary production, it is [500, 1000 kg C m^{-2}];

for x=P$_{ann}$, the total annual precipitation, it is [400, 800 mm];

for x=MTWA, the mean temperature of the warmest month, it is [18, 23°C];

for x=MTCO, the mean temperature of the coldest month, it is [3, 12°C]; the lower limit of 3°C correspond to a minimum mean monthly temperature with no chance to have an absolute daily minimum below -17°C.

for x=α, the actual to potential evapotranspiration ratio, it is [30, 60%].

All factors except those related to NPP$_{trop}$ assume that the vine growth is limited only by their lower values and not by their higher values. Because there is no possible viticulture in the tropics (where temperature is not cold enough for an appropriate dormancy), 1-I$_{NPPtrop}$ is limited by its upper value.

This approach is a static approach as it is based on an equilibrium vegetation model only based on mean state of the climate. The variability of the climate, and then the extreme values of some variables, are not taken into account. We are aware of these limitations, and it is the reason why our interpretations will only concern the potential extension of the viticulture. Other weaknesses of the approach are the impossibility to take into account the diversity of cultivars, the adaptation of grapes to frost

20

and the risk of biotic damage to the grapevines. This is a niche model approach, of the same nature than those used in the literature cited in the beginning of this section. This oversimplified approach has nevertheless the advantage to provide a framework for the past and future trends and to be easily applicable to the past where the data are rather limited.

3 Results

3.1 Paleodata assimilation

From the posterior distributions (Table 9), it appears that the simulated volcanic activity impacts were the strongest during the cold periods (2500, 1300, 700 and 200 yr BP) and rather weak during the dry periods (4200 and 3200 yr BP) and warm periods (2000 and 1000 yr BP). The confidence intervals are significant as they do not overlap. For the present, volcanic and solar activities have no significant impact, which is easily explained by the dominant GHG effect (not used for constraining the assimilation). The impact of solar activity is not clear, as there is no significant difference between cold and warm periods or between the dry and wet periods. The temperature bias (δT independent of the spatial variability) is estimated to be between 0.6 and 1.6°C for the periods between 2500 and 200 yr BP and is not significantly different from zero for the dry periods and for the present. The δP estimates were not significant for any time period. Fig.6 presents the overall correlations between the emulator outputs and the proxy-based reconstructions. A good emulation should be indicated by good coherency of both blue and black lines and a low variance of the dots around the black line. So, the temperature was particularly well simulated by the emulator with a squared correlation (R^2) of 0.75, but with an overestimation of the low temperatures. As expected, precipitation is less well simulated with a significant R^2 of 0.28 with an underestimation of the large (negative or positive) anomalies.

Table 9. Posterior distribution of the parameters. The estimates are given by the best fit and the CI is the 90% confidence intervals calculated on the 10% best fits. Volc index has no units, Solar index is in MeV, T in °C, P, in mm/year.

	Volc	Volc.CI	Solar	Solar.CI	δT	δT.CI	σT	σT.CI	δP	δP.CI	σP	σP.CI
4200	0.1	[0.1, 0.27]	270	[153, 387]	0.3	[-1.7,1.7]	0.8	[0.4,4.7]	-15	[-19,3]	81	[70,81]
3200	0.15	[0.1, 0.33]	267	[190, 387]	-1	[-1.7,1.7]	2.6	[0.4,4.7]	-20	[-20,-7]	81	[66,81]
2500	0.4	[0.4, 0.75]	304	[103, 444]	0.6	[0.2,0.9]	2.1	[1.8,3.5]	16	[-17,18]	25	[5,77]
2000	0.17	[0.1, 0.38]	106	[106, 642]	1.6	[1.1,1.9]	0.9	[0.9,2.8]	-15	[-18,18]	53	[5,75]
1300	0.4	[0.4, 0.76]	324	[121, 452]	1	[0.5,1.3]	1.1	[1.1,2.9]	-9	[-18,18]	45	[6,76]
1000	0.22	[0.1, 0.39]	141	[141, 660]	1.3	[0.9,1.7]	0.9	[0.9,2.7]	-3	[-18,17]	6	[6,76]
700	0.62	[0.4, 0.78]	468	[109, 468]	1.2	[0.8,1.6]	0.9	[0.9,2.7]	-5	[-18,17]	25	[5,76]
200	0.41	[0.4, 0.77]	450	[97, 458]	1.2	[0.7,1.5]	0.3	[0.3,2.6]	4	[-18,17]	49	[5,76]
Present	0.36	[0.15, 0.4]	345	[307, 548]	0.7	[-0.3,1.6]	0.3	[0.2,4.6]	-14	[-18.7,10]	57	[36,79]

Figure 6. Temperature and precipitation anomalies for the 10 Mediterranean boxes estimated by data assimilation versus data reconstructed from proxies. Temperature dots represent the mean annual temperature in the 10 boxes for the 11 periods from 2500 yr BP. until present and precipitation dots represent the total annual precipitation in the two oldest periods (4200 and 3200 yr BP) and in the present. The vertical bars are the 90% confidence intervals (CI). The blue line is the perfect estimate line (R=1), and the black line is the regression line between the simulations and proxy reconstructions.
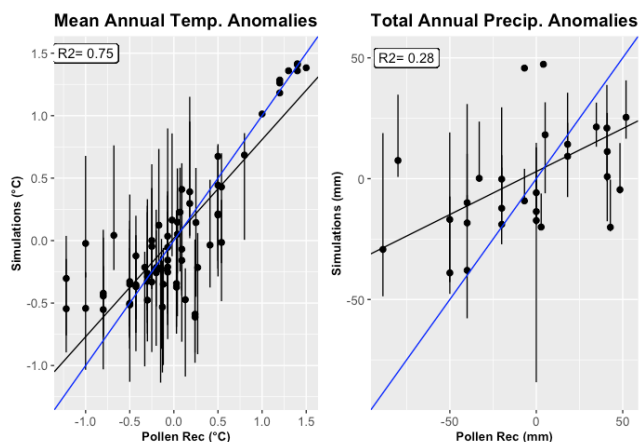
3.2 Application of the emulator to past and future scenarios

This assimilation process was applied to simulate the annual temperature and precipitation for the ten boxes and the 13 time slices/scenarios. The spatial patterns of the reconstructions and simulations are consistent (Fig. 7). Therefore, global forcing variables can drive not only the mean climate evolution but also the spatial patterns reconstructed by the proxy data in the Mediterranean. Volcanic activity seems to be the main driver for the cold periods of the Iron Age (2500 yr BP), the LALIA (1300 yr BP), the LIA (700, 200 yr BP), and for the warm periods of the RCO (2000 yr BP) and MCA (1000 yr BP). The main driver of the present warming and drying (Present time in Fig.7) is GHG forcing. For the 4200 yr BP and 3200 yr BP periods, the volcanic and solar activity drivers do not seem to be plausible explanations for the droughts, at least according to our emulator and likely the ESM's.

Future projections (Fig.8) show general warming for the four scenarios (+1.5C, +2C, +3C, +5C) particularly strong for +3C and +5C scenarios. The local warming is less strong in the areas influenced by the Atlantic Ocean (France and the Iberian

22

Peninsula). For precipitation, the signal is weak for +1.5C and +2C with drier and wetter zones, and clearer for +3C and +5C (all the symbols are triangles, i.e. negative). Combined with the warming, it is undeniable that water stress will increase considerably with +3C and +5C scenarios.

To answer the question of whether volcanic activity can mitigate the impact of high GHG emissions, Fig.8 shows that the temperature distributions of +5CV+ and 5CV- are quite similar, meaning that the cooling effect of volcanoes is relatively low in a large GHG emission scenario. The precipitation distributions of +5CV+ and 5CV- are similar in the western Mediterranean, and +5CV+ produced slightly higher precipitation anomalies than +5CV- in the eastern Mediterranean.

Figure 7. Spatial distribution of the temperature and precipitation anomalies for the past and present time slices. The pairs of symbols are simulations (left symbols) and observations or pollen reconstructions (right symbols). The colors are used for the temperature anomalies. Triangles are used for negative precipitation anomalies and circles for the positive precipitation anomalies. The size of the triangles and circles is proportional to the absolute value of the precipitation anomalies.
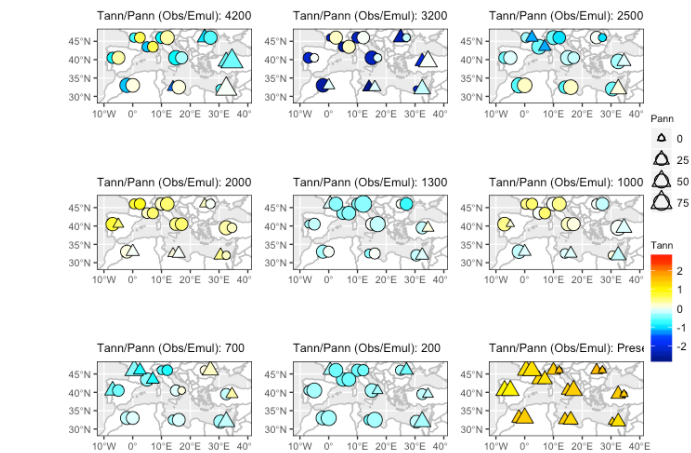
Figure 8. Spatial distribution of the temperature and precipitation anomalies simulated for future time slices (scenarios). The colors are used for the temperature anomalies. Triangles are used for negative precipitation anomalies and circles for positive precipitation anomalies. The size of the triangles and circles is proportional to the absolute value of the precipitation anomalies.

23

Circles = positive anom P / Triangles = negative anom P
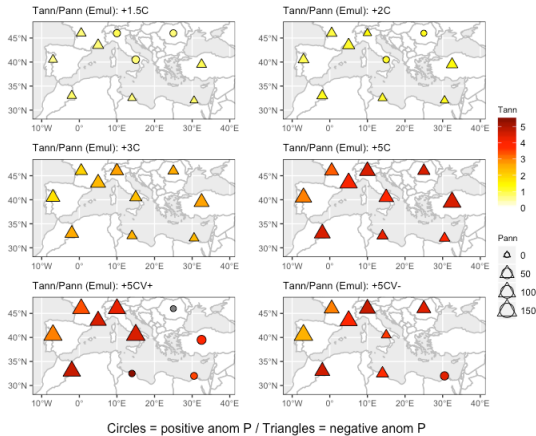
540

3.3 Independent validation

Additional independent validation was completed through comparisons with a tree-ring-based reconstruction of the Palmer Drought Severity Index (PDSI) (Cook et al., 2015) for the last two millennia, when tree-ring data are available. The PDSI reflects the spring-summer soil moisture conditions. We compared this variable with the reconstruction of the E/PE (ratio of

545   actual to potential evapotranspiration in %) variable provided by BIOME4. E/PE is a moisture index which is equal to zero when the soil is fully dry and 100 when it is fully wet. The range of the PDSI index is usually between -6 and 6 units. Negative values correspond to conditions drier than normal. Considering that both indices are not fully similar, a visual comparison shows pretty good agreement (Fig.9). So for 2000 BP, Iberia and Central Europe were wet in both maps, no PDSI data were available for south and east Mediterranean; for 1300 BP, all Europe was dry in both maps except east Spain which was as wet

550   as at 2000 BP; for 1000 BP, the area surrounding the sea was wet except Greece in both maps; for 700 BP: all the area was wetter than 1000 BP in both maps.

Figure 9. Comparison of E/PE reconstructed in this paper with independently reconstructed Palmer Drought Severity Index (PDSI). The PDSI anomalies are based on the 1928-1978 reference period and are reconstructed from tree rings (Cook et al, 555   2015). E/PE is the ratio of actual to potential evapotranspiration obtained from the emulator (in %).

a supprimé: also
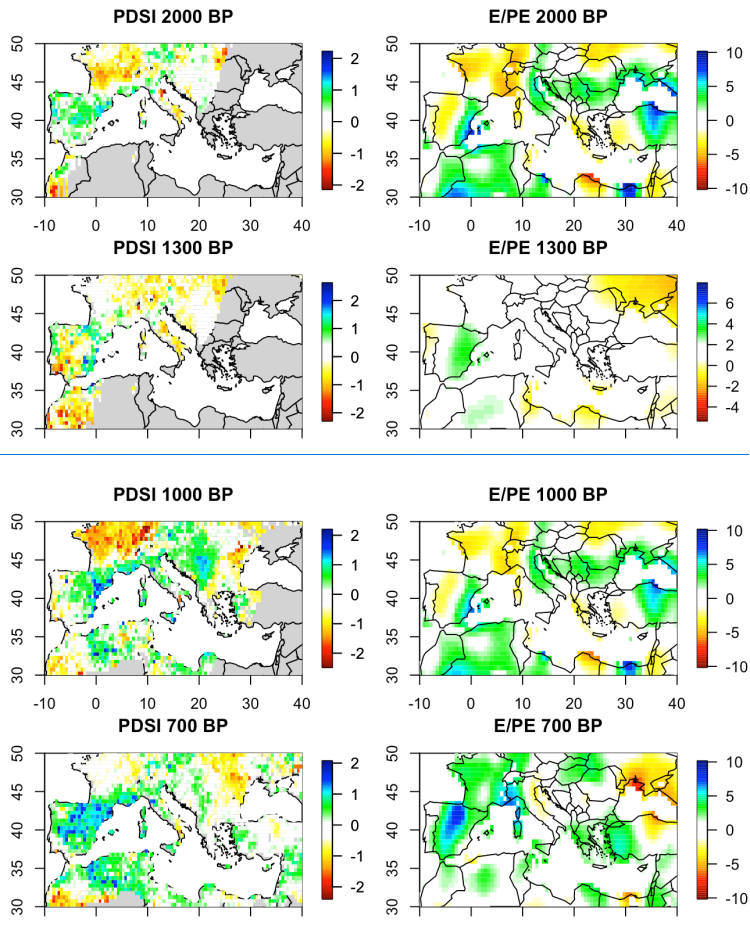
3.4 Evolution of viticulture from the Bronze Age to the end of the 21st century

Applied to the mean climate of 1980-2009, the viticulture index VI approximately reproduces the area in Europe where viticulture is present (Fraga et al., 2013) (Fig.10). As shown in Fig.10a, the simulations give approximately the same limits,

with some noticeable exceptions in Germany, Alpine and Balkan regions, which are likely too continental to pass the MTCO criterion. This is the main limitation of our analysis. The presence of viticulture much depends on local factors such as valleys,

565 slopes, and soil, which are not accounted for in our analysis. More generally, these discrepancies show that our index is not calibrated for continental regions with winters colder than 3°C (in average). This threshold of 3°C is likely overestimated by about 5°C. So, we consider that this index adequately represents the macroclimate of potential vine distribution in western Europe and the Mediterranean region.

The variables needed for the viticulture equation (4) are provided by the emulator for all time slices studied in the past time

570 slices and for future scenarios. The procedure is sketched in Fig.11. We modified the global forcings according to the values of Table 3 for the past and Table 2 for the future and we so simulated, by applying the emulator, viticulture extension maps (Fig.12).

Fig.12 shows that during the dry time slices of 4200 and 3200 yr BP, the suitable areas were located between 34°N and 46°N latitudes. During the cold periods (2500, 1300, 700, and 200 yr BP), they occupied approximately the same area between 34°N

575 and 47°N. During the warmer periods (2000 and 1000 yr BP), the southern limit did not change much, but the northern limit reached 49°N, implying that most of Gaul was suitable for viticulture, as already shown by (Bernigaud et al., 2021). The present map is warmer than the pre-industrial period (200 yr BP slice), which suggests that viticulture is now at its maximum potential extension in four thousand years, up to 51°N. Because of the drier conditions, the southern limit has shifted from 34°N to 35°N. Note that these variations only depend on climate changes, without any consideration of other factors such as

> **a supprimé:** and that we do not consider the

580 type of soils which are very important for the wine quality.

In the future projections, the northern extension of potential viticulture should shift from 51°N (+1.5C scenario) to 53°N (+3C scenario), and even above 55°N (for the +5C scenario). This would allow viticulture to be possible up to Central England, but

> **a supprimé:** more than

it would regress in the south due to stronger water stress. In the Iberian Peninsula, only the Atlantic coast should be suitable for cultivating wine grapes, unless significant irrigation. These projected unfavorable conditions were confirmed by (Fraga et

585 al., 2013) based on other viticulture indices. The 5CV+ and 5CV- scenarios appear quite like the 5C scenario, indicating that the effect of high or low volcanic activities should have a weak effect on the potential distribution of the viticulture in comparison to a strong GHG forcing.

The results are summarized in Fig.13. In the past, only the warm regions of the southern band (29-37°N) had a suitable wine-growing area equivalent to the present. The central geographical band (37-44°N) and the northern one (44-48°N) underwent

590 sudden changes in the viticulture area, first from the cool Iron Age (2500 yr BP) to the RCO (2000 yr BP), and later from the end of the LIA (200 yr BP) to the present. The cold periods are all characterized by a decline in viticulture at latitudes above 37°N. For the future projections, northward displacements are likely to be drastic from +3°C global warming. Viticulture potential will likely disappear from North Africa and is set to decrease drastically in the Iberian Peninsula. In contrast, potential productive areas will likely expand at latitudes above 50°N, in the Balkans and in the Alps, which is a significant change

595 considering that our approach underestimate the grapevine potential of continental climates.

> **a supprimé:** (considering that local climates already enable grape cultivation in some areas with particularly favourable local climates)

26

600 For the two additional scenarios of high emissions combined with extreme volcanic and solar activities, the question is whether an entirely hypothetical set of strong volcanic events could slow down the decline in viticulture in the south. The answer is slightly positive for Spain, Italy, Greece and Turkey (green curve increases for +5CV+ and decreases for +5CV-), but it is negative in North Africa and the Levant (red curve) because the water stress should remain too substantial. The effect is also positive in the northern band and Turkey (the blue and cyan curves increase for +5CV+ and decrease for +5CV-). In all the

605 cases, the effect was clearly too small to compensate for the GHG effect.

Figure 10. Distribution of the wine sites: (a) European wine regions (circles) with the corresponding CompI value for the period of 1980–2009, Fig 1e of Fraga et al. (2013). (b) Simulation using the viticulture index calculated using 1961-1990 climate data.

610
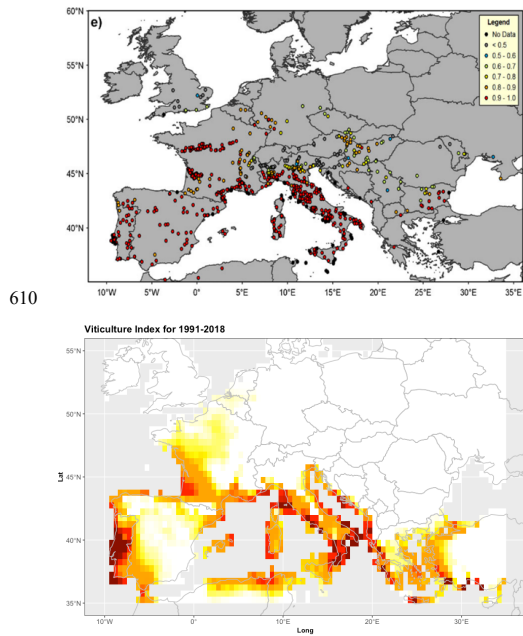
Figure 11. Diagram of the application of the emulator to reconstruct and predict the viticulture extension

Input : global forcings

Output : viticulture extension

Emulator

Application on
historical period

Present (1991-2018)

GHG + δ

Application on
modified global
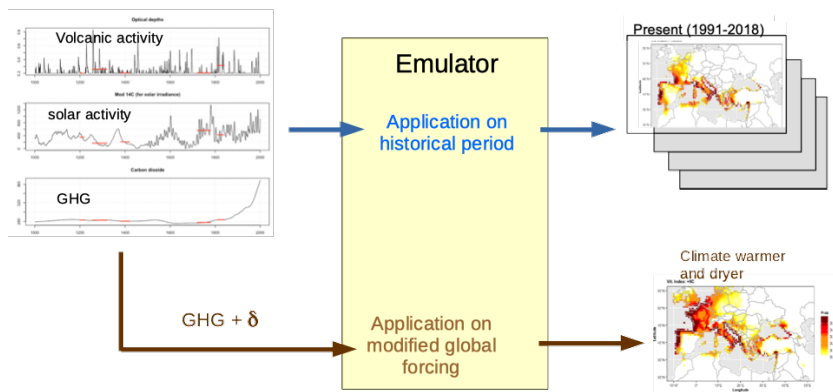forcing

Climate warmer
and dryer

Figure 12. Distribution of the viticulture index (Vit. Index) for several time slices of the past (in yr BP) and future scenarios (expressed as anomalies of global temperature vs pre-industrial reference). The index is labelled VI and is explained in eq.4. White areas indicate where it is impossible to cultivate vine.
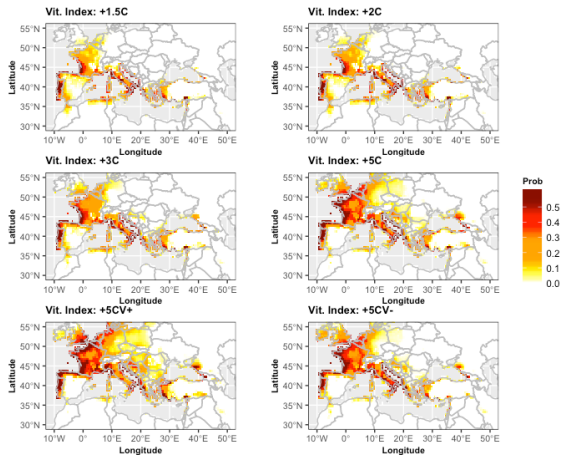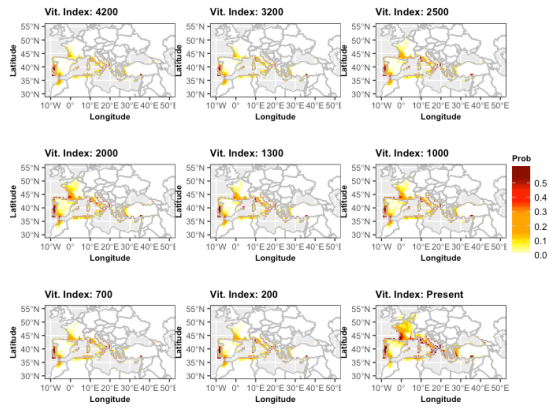
Figure 13. Synthesis of the evolution of viticulture in the Mediterranean area. The curves represent three bands of latitude: southern band with latitude<37°N in red, center band with latitudes between 37 and 44°N in green, northern band with latitudes between 44 and 48°N in blue). The thin lines show the results for the boxes corresponding to Iberian Peninsula, Anatolia and France (definition in Fig.4). The scenarios and time slices are defined in Table 8. The x-axis gives the center of the time slices considered or the future scenario.
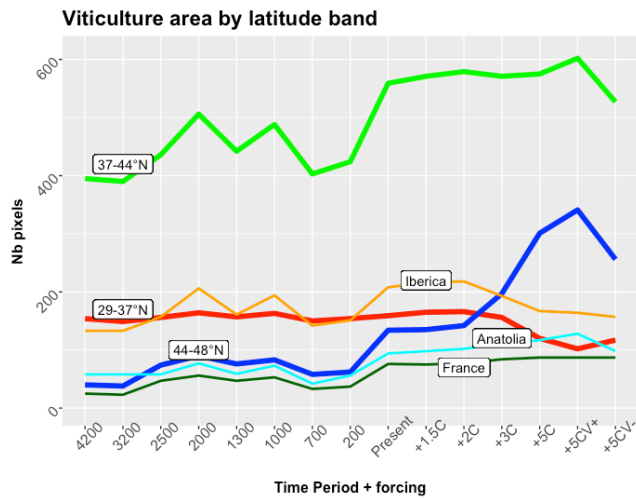
4 Discussion

The discussion considers six points, which concern methodological innovations, contribution to climate science and to viticulture science:

1) We used an emulator approach which recently became popular in the ESM community. In some kind, it has also been used with paleoclimatic data (Crucifix, 2012; Joos et al., 1996), and to emulate a climate-vegetation system (Foley et al., 2015). But this study is the first to use an ensemble of climate models, along with several forcing variables provided by past, present and future states, to project vegetation conditions from global climate drivers. This has involved to solve several technical issues.

2) We showed that the major climatic variations of the last millennia in the Mediterranean Basin can be attributed to volcanic activity, whereas the effects of solar activity were negligible. The effects of volcanic and solar activities have been largely debated, as the reconstruction of temperatures in the last millennium from tree rings has often shown less significant cooling

30

than the model simulations (Mann et al., 2012). A more recent tree-based reconstruction (Stoffel et al., 2015) showed substantial summer cooling after the Samalas eruption in 1257, and that of Tambora in 1816, but less intense than simulated. Luterbacher et al. (2016) showed that solar activity had a relatively weak influence on the European summer temperatures. Thus, our results are in line with the state-of-the-art in the scientific literature.

3) The effect of this volcanic forcing has a clear spatial pattern across the Mediterranean basin. From 2500 yr BP to the present, temperature variations were more significant in the north and in the west than in the southeast (Fig.7). (Fischer et al., 2007) found that northern and western Europe were the coldest and driest areas after an eruption. They also found that southern Europe, North Africa and the Levant have experienced milder and wetter weather than at present. Part of this pattern might be due to regional feedbacks of vegetation on the climate. Some climate model simulations have shown (Reale and Dirmeyer, 2000) that wetter vegetation during the RCO may have induced a northward shift of the intertropical convergence zone during the summer over the African continent with an increase of moisture in North Africa and Iberia, and a decrease in the central Mediterranean (Reale and Shukla, 2000). In the future, the southeast should be relatively less dry and warmer than the northwest especially in summer, which is consistent with our results (Fig.8) (Giorgi and Lionello, 2008).

4) Our simulations of climate change on viticulture are mostly concerned with larger-scale regional production systems since they would require near-full-time engagement of winegrowers with high certainty of production every year, sufficient for speculative trade. For smaller domains and local consumption, it may have also been possible to produce wine under degraded or unstable weather conditions. For example, in England, viticulture continued to be practiced on land owned by the church, even as risks increased due to a wetter climate, with cooler summers and milder winters (Clout, 2013). In most wine regions in western Europe, and particularly in France, the grape harvest dates were advanced after the LIA and particularly after the 1940s (Le Roy Ladurie et al., 2006). For example, from 1945 to the beginning of the 21st century, in Chateauneuf du Pape (Southern Rhone Valley, France) the harvest date advanced on average from October 1 to September 11 (Ganichot, 2002). This change is related to summer warming, but factors related to wine quality, agricultural practices and alcohol content regulation may induce a bias in the interpretation (de Cortázar-Atauri et al., 2010). In the Languedoc region, the potential alcohol content has increased by two degrees from 1984 to 2013 (van Leeuwen and Darriet, 2016). Even if the alcohol content does not exactly reflect the grape yields, earlier harvest dates with a higher sugar content are clearly related to improved conditions of grape cultivation since the LIA which is also related to increased productivity. Another climate-sensitive symbol of Mediterranean agriculture is the olive trees. (Moriondo et al., 2013) found three characteristic periods in olive-growing, namely: the RCO (300 BCE to 400 CE) and the MCA (900 CE to 1200 CE) during which olive-growing areas expanded northward, and the LIA (1400 CE to 1900 CE) during which a contraction was reported. This is consistent with the variations in viticulture, at least in western Europe and Mediterranean area as our VI index is not properly calibrated for strongly continental climates.

5) Major difficulties are forecast for 21st century viticulture in Spain and North Africa. These are particularly important for global warming levels of +3°C and more. (Caffarra and Eccel, 2011) showed that the projected warming should make some mountain sites at approximately 1000 m climatically suitable for viticulture before the end of this century. The MCA limit will

31

680 certainly be passed. However, other factors could become limiting, such as excessively mild winters that enable pest attacks and infections, lack of expertise in vine growing and wine making, and products that are more expensive than the current Mediterranean wines (Clout, 2013). Other limitations are the extreme events (late frost, flooding). More frequent and more intense heatwaves will no longer be favorable to viticulture at the present southern Mediterranean limit of its niche. These factors are not considered in our approach. A recent study considering the grapes varieties showed (Sgubin et al., 2022) that,

685 for global temperature anomalies below 2°C, the mean relative area loss was estimated to be 3.9%/°C, while for higher values of global warming this loss trend is estimated to be a much larger rate of 17.1%/°C. This confirms the existence of a safe limit below 2°C of global warming for the European winemaking sector, above which adaptation might become far more challenging.

6) It is not very likely that intense volcanic activity could slow down this decline, because (despite of the many other negative

690 consequences of such events) the beneficial climatic effects of this activity would be highest in regions with increased wine growing potential under global warming (Turkey, northern Europe, the Alps, and the Balkans) and negligible in North Africa. IPCC has assessed the literature concerning the question of whether volcanic eruptions could be analogous for geoengineering proposals for climate mitigation (Myhre et al., 2013). Independent of their possible negative side effects, solar radiation modification (SRM), consisting in injecting sulfur aerosols in the stratosphere like a volcano does, is likely not an efficient

695 technique to cool the atmosphere. Indeed, our results show that a very strong volcanic activity, even accompanied by a low solar activity, should not have any significant effects on viticulture extension in comparison to the radiative forcing from anthropogenic GHG emissions.

5 Conclusion

We demonstrated the efficiency of a statistical emulator based on multiple ESMs and calibrated over a large range of forcing

700 and climate states to link the production of a regionally important crop (grapes) to global climate forcing variables. There are two main methodological innovations: (i) past climate simulations are used together with future ones to calibrate a robust emulator, (ii) this emulator is independent of any single model because it captures what is common among all the available model simulations. But it remains an emulator which capture no more than the information contained in the ESMs.

Using it on past time slices, we showed that volcanic activity is a good predictor of the past temperature variations in the

705 Mediterranean Basin and consequently of the viticulture productivity. During the warm phases of the historical times (The Roman Climate Optimum and the Medieval Climate Anomaly), characterized by a low volcanic activity, the viticulture area has shifted northward from 47°N to 49°N. This historical limit has already passed at the present time as it has already shifted to 51°N and with a global warming of +3°C, it should pass the 53°N limit. Even if, in the warm periods of the past, North African and Iberian farmers never had real difficulties in cultivating grapes, they will meet large difficulties with a global

710 warming of +3°C or more, except on their Atlantic margin. Moreover, our sensitivity experiments show that even an intense volcanic activity is not sufficient to stop this decline.

Open access:

All data, codes, and materials used in the analyses are available at https://github.com/douane7/C5P3_B4_emul.git.

725 **References**

Allen, M. R., Dube, O. P., Solecki, W., Aragón-Durand, F., Cramer, W., Humphreys, S., Kainuma, M., Kala, J., Mahowald, N., Mulugetta, Y., Perez, R., Wairiu, M., and Zickfeld, K.: Framing and Context, in: Global Warming of 1.5°C. An IPCC Special Report on the impacts of global warming of 1.5°C above pre-industrial levels and related global greenhouse gas emission pathways, in the context of strengthening the global response to the threat of climate change, edited by: Masson-
730 Delmotte, V., Zhai, P., Pörtner, H.-O., Roberts, D., Skea, J., Shukla, P. R., Pirani, A., Moufouma-Okia, W., Péan, C., Pidcock, R., Connors, S., Matthews, J. B. R., Chen, Y., Zhou, X., Gomis, M. I., Lonnoy, E., Maycock, T., Tignor, M., and T. Water, In press, 49–92, 2018.

Amara, R.: Views on futures research methodology, Futures, 23, 645–649, https://doi.org/10.1016/0016-3287(91)90085-G, 1991.

735 Berger, A. and Loutre, M. F.: Insolation values for the climate of the last 10,000,000 years, Quat. Sci. Rev., 10, 297–317, 1991.

Bernigaud, N., Bondeau, A., and Guiot, J.: Understanding the development of viticulture in Roman Gaul during and after the Roman climate optimum: The contribution of spatial analysis and agro-ecosystem modeling, J. Archaeol. Sci. Reports, 38, 1–9, https://doi.org/10.1016/j.jasrep.2021.103099, 2021.

740 Bouby, L., Marinval, P., and Terral, J.-F.: From secondary to speculative ProductIon? the Protohistory history of viticulture in Southern France, in: Plants and People: choices and diversity through time, edited by: Chevalier, A., Marinova, E., and Chocarro, L. P., Oxbow Book, London & Philadelphia, 175–181, https://doi.org/10.2307/1309151, 2014.

Bouby, L., Wales, N., Jalabadze, M., Rusishvili, N., Bonhomme, V., Ramos-Madrigal, J., Evin, A., Ivorra, S., Lacombe, T., Pagnoux, C., Boaretto, E., Gilbert, M. T. P., Bacilieri, R., Lordkipanidze, D., and Maghradze, D.: Tracking the history of grape
745 cultivation in Georgia combining geometric morphometrics and ancient DNA, Veg. Hist. Archaeobot., 30, 63–76, https://doi.org/10.1007/s00334-020-00803-0, 2021.

Bounceur, N., Crucifix, M., and Wilkinson, R. D.: Global sensitivity analysis of the climate-vegetation system to astronomical forcing: An emulator-based approach, Earth Syst. Dyn., 6, 205–224, https://doi.org/10.5194/esd-6-205-2015, 2015.

Braconnot, P., Harrison, S. P., Kageyama, M., Bartlein, P. J., Masson-Delmotte, V., Abe-Ouchi, A., Otto-Bliesner, B., and Zhao, Y.: Evaluation of climate models using palaeoclimatic data, Nat. Clim. Chang., 2, 417–424, https://doi.org/10.1038/nclimate1456, 2012.

Brayshaw, D. J., Hoskins, B., and Black, E.: Some physical drivers of changes in the winter storm tracks over the North Atlantic and Mediterranean during the Holocene., Philos. Trans. A. Math. Phys. Eng. Sci., 368, 5185–5223, https://doi.org/10.1098/rsta.2010.0180, 2010.

Brown, A. G., Meadows, I., Turner, S. D., and Mattingley, D.: Roman vineyards in Britain: stratigraphic and palynological data from Wollaston in the Nene Valley, England., Antiquity, 75, 745–757, 2001.

Brun, J.-P.: 15. Viticulture et oléiculture en Gaule, in: Comment les Gaules devinrent romaines, edited by: Pierre Ouzoulias, La Découverte, Paris, 231–253, 2010.

Brunsdon, C., Fotheringham, S., and Charlton, M.: Geographically weighted regression - Modelling spatial non-stationarity, J. R. Stat. Soc. Ser. D Stat., 47, 431–443, https://doi.org/10.1111/1467-9884.00145, 1998.

Büntgen, U., Tegel, W., Nicolussi, K., McCormick, M., Frank, D., Trouet, V., Kaplan, J. O., Herzig, F., Heussner, K.-U., Wanner, H., Luterbacher, J., and Esper, J.: 2500 years of European climate variability and human susceptibility., Science, 331, 578–582, https://doi.org/10.1126/science.1197175, 2011.

Büntgen, U., Myglan, V. S., Ljungqvist, F. C., Mccormick, M., Cosmo, N. Di, Sigl, M., Jungclaus, J., Wagner, S., Krusic, P. J., Esper, J., Kaplan, J. O., Vaan, M. A. C. De, Luterbacher, J., Wacker, L., and Tegel, W.: Cooling and societal change during the Late Antique Little Ice Age from 536 to around 660 AD, Nat. Geosci., https://doi.org/10.1038/NGEO2652, 2016.

Caffarra, A. and Eccel, E.: Projecting the impacts of climate change on the phenology of grapevine in a mountain area, Aust. J. Grape Wine Res., 17, 52–61, https://doi.org/10.1111/j.1755-0238.2010.00118.x, 2011.

Castruccio, S., McInerney, D. J., Stein, M. L., Crouch, F. L., Jacob, R. L., and Moyer, E. J.: Statistical emulation of climate model projections based on precomputed GCM runs, J. Clim., 27, 1829–1844, https://doi.org/10.1175/JCLI-D-13-00099.1, 2014.

Chandler, R. E.: Exploiting strength, discounting weakness: Combining information from multiple climate simulators, Philos. Trans. R. Soc. A Math. Phys. Eng. Sci., 371, https://doi.org/10.1098/rsta.2012.0388, 2013.

Clout, H.: An Overview of the Fluctuating Fortunes of Viticulture in England and Wales, EchoGeo, 23, https://doi.org/10.4000/echogeo.13333, 2013.

Cook, E. R., Seager, R., Kushnir, Y., Briffa, K. R., Büntgen, U., Frank, D., Krusic, P. J., Tegel, W., Schrier, G. Vander, Andreu-Hayles, L., Baillie, M., Baittinger, C., Bleicher, N., Bonde, N., Brown, D., Carrer, M., Cooper, R., Eùfar, K., DIttmar, C., Esper, J., Griggs, C., Gunnarson, B., Günther, B., Gutierrez, E., Haneca, K., Helama, S., Herzig, F., Heussner, K. U., Hofmann, J., Janda, P., Kontic, R., Köse, N., Kyncl, T., Levaniè, T., Linderholm, H., Manning, S., Melvin, T. M., Miles, D., Neuwirth, B., Nicolussi, K., Nola, P., Panayotov, M., Popa, I., Rothe, A., Seftigen, K., Seim, A., Svarva, H., Svoboda, M., Thun, T., Timonen, M., Touchan, R., Trotsiuk, V., Trouet, V., Walder, F., Wany, T., Wilson, R., and Zang, C.: Old World megadroughts and pluvials during the Common Era, Sci. Adv., 1, 37, https://doi.org/10.1126/sciadv.1500561, 2015.

34

de Cortázar-Atauri, I. G., Daux, V., Garnier, E., Yiou, P., Viovy, N., Seguin, B., Boursiquot, J. M., Parker, A. K., van Leeuwen, C., and Chuine, I.: Climate reconstructions from grape harvest dates: Methodology and uncertainties, Holocene, 20, 599–608, https://doi.org/10.1177/0959683609356585, 2010.

785 Crowley, T. J. and Unterman, M. B.: Technical details concerning development of a 1200 yr proxy index for global volcanism, Earth Syst. Sci. Data, 5, 187–197, https://doi.org/10.5194/essd-5-187-2013, 2013.

Crucifix, M.: Traditional and novel approaches to palaeoclimate modelling, Quat. Sci. Rev., 57, 1–16, https://doi.org/10.1016/j.quascirev.2012.09.010, 2012.

790 Finné, M., Holmgren, K., Sundqvist, H. S., Weiberg, E., and Lindblom, M.: Climate in the eastern Mediterranean, and adjacent regions, during the past 6000 years - A review, J. Archaeol. Sci., 38, 3153–3173, https://doi.org/10.1016/j.jas.2011.05.007, 2011.

Fischer, E. a., Luterbacher, J., Zorita, E., Tett, S. F. B., Casty, C., and Wanner, H.: European climate response to tropical volcanic eruptions over the last half millennium, Geophys. Res. Lett., 34, 1–6, https://doi.org/10.1029/2006GL027992, 2007.

795 Foley, A. M., Holden, P. B., Edwards, N. R., Mercure, J.-F., Salas, P., Pollitt, H., and Chewpreecha, U.: Climate model emulation in an integrated assessment framework: a case study for mitigation policies in the electricity sector, Earth Syst. Dyn. Discuss., 6, 1277–1308, https://doi.org/10.5194/esdd-6-1277-2015, 2015.

Fraga, H., Malheiro, A. C., Moutinho-Pereira, J., and Santos, J. A.: Future scenarios for viticultural zoning in Europe: Ensemble projections and uncertainties, Int. J. Biometeorol., 57, 909–925, https://doi.org/10.1007/s00484-012-0617-8, 2013.

800 Franklin, J., Serra-Diaz, J. M., Syphard, A. D., and Regan, H. M.: Global change and terrestrial plant community dynamics, Proc. Natl. Acad. Sci. U. S. A., 113, 3725–3734, https://doi.org/10.1073/pnas.1519911113, 2016.

Frieler, K., Lange, S., Piontek, F., Reyer, C. P. O., Schewe, J., Warszawski, L., Zhao, F., Chini, L., Denvil, S., Emanuel, K., Geiger, T., Halladay, K., Hurtt, G., Mengel, M., Murakami, D., Ostberg, S., Popp, A., and Riva, R.: Assessing the impacts of 1.5 ◦ C global warming – simulation protocol of the Inter-Sectoral Impact Model Intercomparison Project (ISIMIP2b),
805 Geosci. Model Dev., 10, 4321–4345, https://doi.org/10.5194/gmd-10-4321-2017, 2017.

Fuks, D., Ackermann, O., Ayalon, A., Bar-Matthews, M., Bar-Oz, G., Levi, Y., Maeir, A. M., Weiss, E., Zilberman, T., and Safrai, Z.: Dust clouds, climate change and coins: consiliences of palaeoclimate and economy in the Late Antique southern Levant, Levant, 49, 205–223, https://doi.org/10.1080/00758914.2017.1379181, 2017.

Ganichot, B.: Évolution de la date des vendanges dans les Côtes du Rhône méridionales, in: Rencontres rhodaniennes, 38–41,
810 2002.

Giorgi, F. and Lionello, P.: Climate change projections for the Mediterranean region, Glob. Planet. Change, 63, 90–104, https://doi.org/10.1016/j.gloplacha.2007.09.005, 2008.

Goosse, H., Guiot, J., Mann, M. E. M. E., Dubinkina, S., and Sallaz-Damaz, Y.: The medieval climate anomaly in Europe: Comparison of the summer and annual mean signals in two reconstructions and in simulations with data assimilation, Glob.
815 Planet. Change, 84–85, 35–47, https://doi.org/10.1016/j.gloplacha.2011.07.002, 2012.

Grouillet, B., Ruelland, D., Ayar, P. V., and Vrac, M.: Sensitivity analysis of runoff modeling to statistical downscaling models

in the western Mediterranean, Hydrol. Earth Syst. Sci., 20, 1031–1047, https://doi.org/10.5194/hess-20-1031-2016, 2016.

Guiot, J. and Cramer, W.: Climate change: The 2015 Paris Agreement thresholds and Mediterranean basin ecosystems, Science (80-.)., 354, 4528–4532, https://doi.org/10.1126/science.aah5015, 2016.

820 Guiot, J. and Kaniewski, D.: The Mediterranean Basin and Southern Europe in a warmer world: What can we learn from the past?, 1–16 pp., https://doi.org/10.3389/feart.2015.00028, 2015.

Guiot, J., Torre, F., Jolly, D., Peyron, O., Boreux, J. J. J., Cheddadi, R., Borreux, J. J., and Cheddadi, R.: Inverse vegetation modeling by Monte Carlo sampling to reconstruct paleoclimate under changed precipitation seasonality and CO2 conditions: application to glacial climate in Mediterranean region, Ecol. Modell., 127, 119–140, https://doi.org/10.1016/S0304-

825 3800(99)00219-7, 2000.

Hargreaves, J. and Annan, J.: Assimilation of paleo-data in simple Earth system model, Clim. Dyn., 19, 371–381, https://doi.org/10.1007/s00382-002-0241-0, 2002.

Holzhauser, H., Magny, M., and Zumbuhl, H. J.: Glacier and lake-level variations in west-central Europe over the last 3500 years, HOLOCENE, 15, 789–801, https://doi.org/10.1191/0959683605hl853ra, 2005.

830 Howell, S. G.: Sustainable Grape Productivity and the Growth-Yield Relationship, Am. J. Enol. Vitic., 52, 165–174, 2001.

Izdebski, A., Holmgren, K., Weiberg, E., Stocker, S. R., Buntgen, U., Florenzano, A., Gogou, A., Leroy, S. A. G., Luterbacher, J., Martrat, B., Masi, A., Mercuri, A. M., Montagna, P., Sadori, L., Schneider, A., Sicre, M. A., Triantaphyllou, M., and Xoplaki, E.: Realising consilience: How better communication between archaeologists, historians and natural scientists can transform the study of past climate change in the Mediterranean, Quat. Sci. Rev., 136,

835 https://doi.org/10.1016/j.quascirev.2015.10.038, 2016.

Joos, F., Bruno, M., Fink, R., Siegenthaler, U., Stocker, T., LeQuere, C., and Sarmiento, J. L.: An efficient and accurate representation of complex oceanic and biospheric models of anthropogenic carbon uptake, Tellus, 48B, 397–417, 1996.

Kaniewski, D., Guiot, J., and Van Campo, E.: Drought and societal collapse 3200years ago in the Eastern Mediterranean: A review, Wiley Interdiscip. Rev. Clim. Chang., 6, 369–382, https://doi.org/10.1002/wcc.345, 2015.

840 Kaniewski, D., Marriner, N., Cheddadi, R., Guiot, J., Campo, E. Van, Sabatier-toulouse, P., and Laboratoire, E.: The 4.2 ka BP event in the Levant, Clim. Past, 14, 1529–1542, 2018.

Kaplan, J. O., Prentice, I. C., and Buchmann, N.: The stable carbon isotope composition of the terrestrial biosphere: Modeling at scales from the leaf to the globe, Global Biogeochem. Cycles, 16, https://doi.org/10.1029/2001gb001403, 2002.

Kay, J. E., Deser, C., Phillips, A., Mai, A., Hannay, C., Strand, G., Arblaster, J. M., Bates, S. C., Danabasoglu, G., Edwards,

845 J., Holland, M., Kushner, P., Lamarque, J. F., Lawrence, D., Lindsay, K., Middleton, A., Munoz, E., Neale, R., Oleson, K., Polvani, L., and Vertenstein, M.: The Community Earth System Model (CESM) Large Ensemble Project: A Community Resource for Studying Climate Change in the Presence of Internal Climate Variability, Bull. Am. Meteorol. Soc., https://doi.org/10.1175/BAMS-D-13-00255.1, 2014.

Kennedy, M. C. and O'Hagan, A.: Predicting the output from a complex computer code when fast approximations are

850 available, Biometrika, 87, 1–13, https://doi.org/10.1093/biomet/87.1.1, 2000.

Klein Goldewijk, K., Beusen, A., Van Drecht, G., and De Vos, M.: The HYDE 3.1 spatially explicit database of human-induced global land-use change over the past 12,000 years, Glob. Ecol. Biogeogr., 20, 73–86, https://doi.org/10.1111/j.1466-8238.2010.00587.x, 2011.

855 Lavigne, F., Degeai, J.-P., Komorowski, J.-C., Guillet, S., Robert, V., Lahitte, P., Oppenheimer, C., Stoffel, M., Vidal, C. M., Surono, Pratomo, I., Wassmer, P., Hajdas, I., Hadmoko, D. S., and de Belizal, E.: Source of the great A.D. 1257 mystery eruption unveiled, Samalas volcano, Rinjani Volcanic Complex, Indonesia, Proc. Natl. Acad. Sci., 110, 16742–16747, https://doi.org/10.1073/pnas.1307520110, 2013.

van Leeuwen, C. and Darriet, P.: The Impact of Climate Change on Viticulture and Wine Quality, J. Wine Econ., 11, 150–167, https://doi.org/10.1017/jwe.2015.21, 2016.

860 Levavasseur, G., Vrac, M., Roche, D. M., Paillard, D., Martin, A., and Vandenberghe, J.: Present and LGM permafrost from climate simulations: Contribution of statistical downscaling, Clim. Past, 7, 1225–1246, https://doi.org/10.5194/cp-7-1225-2011, 2011.

Leveau, P.: « Les conditions environnementales dans le nord de l'Afrique à l'époque romaine. Contribution historiographique à l'histoire du climat et des relations homme / milieu, in: Sociétés et climats dans l'Empire romain. Pour une perspective 865 historique et systémique de la gestion des ressources en eau dans l'Empire romain., edited by: Hermon, E., Editoriale Scientifica, Naples, 309–348, 2009.

Lu, B., Charlton, M., Harris, P., and Fotheringham, A. S.: Geographically weighted regression with a non-Euclidean distance metric: A case study using hedonic house price data, Int. J. Geogr. Inf. Sci., 28, 660–681, https://doi.org/10.1080/13658816.2013.865739, 2014.

870 Luterbacher, J., Werner, J. P. P., Smerdon, J. E. E., Fernández-Donado, L., González-Rouco, F. J. J., Barriopedro, D., Ljungqvist, F. C. C., Büntgen, U., Zorita, E., Wagner, S., Esper, J., McCarroll, D., Toreti, A., Frank, D., Jungclaus, J. H. H., Barriendos, M., Bertolin, C., Bothe, O., Brázdil, R., Camuffo, D., Dobrovolný, P., Gagen, M., García-Bustamante, E., Ge, Q., Gómez-Navarro, J. J. J., Guiot, J., Hao, Z., Hegerl, G. C. C., Holmgren, K., Klimenko, V. V. V, Martín-Chivelet, J., Pfister, C., Roberts, N., Schindler, A., Schurer, A., Solomina, O., Von Gunten, L., Wahl, E., Wanner, H., Wetter, O., Xoplaki, E., 875 Yuan, N., Zanchettin, D., Zhang, H., and Zerefos, C.: European summer temperatures since Roman times, Environ. Res. Lett., 11, 024001, https://doi.org/10.1088/1748-9326/11/2/024001, 2016.

Magny, M., Combourieu-Nebout, N., De Beaulieu, J. L., Bout-Roumazeilles, V., Colombaroli, D., Desprat, S., Francke, A., Joannin, S., Ortu, E., Peyron, O., Revel, M., Sadori, L., Siani, G., Sicre, M. A., Samartin, S., Simonneau, A., Tinner, W., Vanniere, B., Wagner, B., Zanchetta, G., Anselmetti, F., Brugiapaglia, E., Chapron, E., Debret, M., Desmet, M., Didier, J., 880 Essallami, L., Galop, D., Gilli, A., Haas, J. N., Kallel, N., Millet, L., Stock, A., Turon, J. L., and Wirth, S.: North-south palaeohydrological contrasts in the central mediterranean during the holocene: Tentative synthesis and working hypotheses, Clim. Past, 9, 2043–2071, https://doi.org/10.5194/cp-9-2043-2013, 2013.

Malheiro, A. C., Santos, J. A., Fraga, H., and Pinto, J. G.: Climate change scenarios applied to viticultural zoning in Europe, Clim. Res., 43, 163–177, https://doi.org/10.3354/cr00918, 2010.

885 Mann, M. E., Fuentes, J. D., and Rutherford, S.: Underestimation of volcanic cooling in tree-ring-based reconstructions of hemispheric temperatures, Nat. Geosci., 5, 202–205, https://doi.org/10.1038/ngeo1394, 2012.

Mccormick, M., Büntgen, U., Cane, M. A., Cook, E. R., Harper, K., Huybers, P., Litt, T., Manning, S. W., Mayewski, P. A., More, A. F. M., Nicolussi, K., and Tegel, W.: Climate Change During & After the Roman Empire, J. Interdiscip. Hist., xliii, 169–220, https://doi.org/10.1162/JINH_a_00379, 2012.

890 Moriondo, M., Trombi, G., Ferrise, R., Brandani, G., Dibari, C., Ammann, C. M., Lippi, M. M., and Bindi, M.: Olive trees as bio-indicators of climate evolution in the Mediterranean Basin, Glob. Ecol. Biogeogr., 22, https://doi.org/10.1111/geb.12061, 2013.

Moss, R. H., Edmonds, J. a, Hibbard, K. a, Manning, M. R., Rose, S. K., van Vuuren, D. P., Carter, T. R., Emori, S., Kainuma, M., Kram, T., Meehl, G. a, Mitchell, J. F. B., Nakicenovic, N., Riahi, K., Smith, S. J., Stouffer, R. J., Thomson, A. M., Weyant,
895 J. P., and Wilbanks, T. J.: The next generation of scenarios for climate change research and assessment., Nature, 463, 747–56, https://doi.org/10.1038/nature08823, 2010.

Muscheler, R., Joos, F., Beer, J., Müller, S. A., Vonmoos, M., and Snowball, I.: Solar activity during the last 1000yr inferred from radionuclide records, Quat. Sci. Rev., 26, 82–97, https://doi.org/https://doi.org/10.1016/j.quascirev.2006.07.012, 2007.

Myhre, G., Shindell, D., Bréon, F.-M., Collins, W., Fuglestvedt, J., Huang, J., Koch, D., Lamarque, J.-F., Lee, D., Mendoza,
900 B., Nakajima, T., Robock, A., Stephens, G., Takemura, T., and Zhang, H.: Anthropogenic and Natural Radiative Forcing, in: Climate Change 2013: The Physical Science Basis. Contribution of Working Group I to the Fifth Assessment Report of the Intergovernmental Panel on Climate Change, edited by: Stocker, T. F., Qin, D., Plattner, G.-K., Tignor, M., Allen, S. K., Boschung, J., Nauels, A., Xia, Y., Bex, V., and Midgley, P. M., Cambridge University Press, Cambridge, United Kingdom and New York, NY, USA, 659–740, https://doi.org/10.1017/CBO9781107415324.018, 2013.

905 Neumann, J. . and Parpola, S. .: Climatic Change and the Eleventh-Tenth-Century Eclipse of Assyria and Babylonia, J. Near East. Stud., 46, 161–182, 1987.

New, M., Lister, D., Hulme, M., and Makin, I.: A high-resolution data set of surface climate over global land areas, Clim. Res., 21, 1–25, https://doi.org/10.3354/cr021001, 2002.

Prentice, I. C., Cramer, W., Harrison, S. P., Leemans, R., Monserud, R. A., and Solomon, A. M.: A global biome model based
910 on plant physiology and dominance, soil properties and climate, J. Biogeogr., 19, 117–134, 1992.

Reale, O. and Dirmeyer, P.: Modeling the effects of vegetation on Mediterranean climate during the Roman Classical Period. Part I: Climate history and model sensitivity, Glob. Planet. Change, 25, 163–184, https://doi.org/10.1016/S0921-8181(00)00002-3, 2000.

Reale, O. and Shukla, J.: Modeling the effects of vegetation on Mediterranean climate during the Roman Classical Period: Part
915 II. Model simulation, Glob. Planet. Change, 25, 185–214, https://doi.org/10.1016/S0921-8181(00)00003-5, 2000.

Roberts, N., Brayshaw, D., Kuzucuoğlu, C., Perez, R., and Sadori, L.: The mid-Holocene climatic transition in the Mediterranean: causes and consequences, The Holocene, 21, 3–13, https://doi.org/10.1177/0959683610388058, 2011.

Rougier, J. and Goldstein, M.: Climate Simulators and Climate Projections, Annu. Rev. Stat. Its Appl., 1, 103–123,

https://doi.org/10.1146/annurev-statistics-022513-115652, 2014.

920 Le Roy Ladurie, E., Daux, V., and Luterbacher, J.: Vignes et vendanges des XIV-XXIe siècles, Hist. économie société, 25e année, 421–436, https://doi.org/10.3917/hes.063.0421, 2006.

Santos, J. A., Malheiro, A. C., Pinto, J. G., and Jones, G. V.: Macroclimate and viticultural zoning in Europe: Observed trends and atmospheric forcing, Clim. Res., 51, 89–103, https://doi.org/10.3354/cr01056, 2012.

Sgubin, G., Swingedouw, D., Mignot, J., Alan, G., Benjamin, G., Harilaos, B., Thomas, L., Pieri, P., García, I., Ollat, A. N., 925 and Leeuwen, C. Van: Linear loss of suitable wine regions over Europe in response to increasing global warming, Glob. Chang. Biol., 1–19, https://doi.org/10.1111/gcb.16493, 2022.

Sharifi, A., Pourmand, A., Canuel, E. A., Ferer-Tyler, E., Peterson, L. C., Aichner, B., Feakins, S. J., Daryaee, T., Djamali, M., Beni, A. N., Lahijani, H. A. K., and Swart, P. K.: Abrupt climate variability since the last deglaciation based on a high-resolution, multi-proxy peat record from NW Iran: The hand that rocked the Cradle of Civilization?, Quat. Sci. Rev., 123, 215– 930 230, https://doi.org/10.1016/j.quascirev.2015.07.006, 2015.

Sigl, M., Winstrup, M., McConnell, J. R., Welten, K. C., Plunkett, G., Ludlow, F., Büntgen, U., Caffee, M., Chellman, N., Dahl-Jensen, D., Fischer, H., Kipfstuhl, S., Kostick, C., Maselli, O. J., Mekhaldi, F., Mulvaney, R., Muscheler, R., Pasteris, D. R., Pilcher, J. R., Salzer, M., Schüpbach, S., Steffensen, J. P., Vinther, B. M., and Woodruff, T. E.: Timing and climate forcing of volcanic eruptions for the past 2,500 years., Nature, 523, 543–9, https://doi.org/10.1038/nature14565, 2015.

935 Stoffel, M., Khodri, M., Corona, C., Guillet, S., Poulain, V., Bekki, S., Guiot, J., Luckman, B. H., Oppenheimer, C., Lebas, N., Beniston, M., and Masson-Delmotte, V.: Estimates of volcanic-induced cooling in the Northern Hemisphere over the past 1,500 years, Nat. Geosci., 8, 784–788, https://doi.org/10.1038/ngeo2526, 2015.

Strassmann, K. M. and Joos, F.: The Bern Simple Climate Model (BernSCM) v1.0: An extensible and fully documented open-source re-implementation of the Bern reduced-form model for global carbon cycle-climate simulations, Geosci. Model Dev., 940 11, 1887–1908, https://doi.org/10.5194/gmd-11-1887-2018, 2018.

Su, B., Huang, J., Gemmer, M., Jian, D., Tao, H., Jiang, T., and Zhao, C.: Statistical downscaling of CMIP5 multi-model ensemble for projected changes of climate in the Indus River Basin, Atmos. Res., 178, 138–149, https://doi.org/10.1016/j.atmosres.2016.03.023, 2016.

Taylor, K. E., Stouffer, R. J., and Meehl, G. A.: An overview of CMIP5 and the experiment design, Bull. Am. Meteorol. Soc., 945 93, 485–498, https://doi.org/10.1175/BAMS-D-11-00094.1, 2012.

Telelis, I.: Climatic Fluactions in the Eastern Mediterranean and the Middle East AD 300-1500 from Byzantine Documentary and Proxy Physical Paleoclimatic Evidence - A Comparison, Jahrb. der Österreichischen Byzantinistik, 58, 167–208, https://doi.org/10.1553/joeb58s167, 2008.

Terral, J.-F., Tabard, E., Bouby, L., Ivorra, S., Pastor, T., Figueiral, I., Picq, S., Chevance, J.-B., Jung, C., Fabre, L., Tardy, C., 950 Compan, M., Bacilieri, R., Lacombe, T., and This, P.: Evolution and history of grapevine (Vitis vinifera) under domestication: new morphometric perspectives to understand seed domestication syndrome and reveal origins of ancient European cultivars, Ann. Bot., 105, 443–455, https://doi.org/10.1093/aob/mcp298, 2010.

Tonietto, J. and Carbonneau, A.: A multicriteria climatic classification system for grape-growing regions worldwide, Agric. For. Meteorol., 124, 81–97, https://doi.org/10.1016/j.agrformet.2003.06.001, 2004.

955 Tran, G. T., Oliver, K. I. C., Sóbester, A., Toal, D. J. J., Holden, P. B., Marsh, R., Challenor, P., and Edwards, N. R.: Building a traceable climate model hierarchy with multi-level emulators, Adv. Stat. Climatol. Meteorol. Oceanogr., 2, 17–37, https://doi.org/10.5194/ascmo-2-17-2016, 2016.

van Vuuren, D. P., Isaac, M., Kundzewicz, Z. W., Arnell, N., Barker, T., Criqui, P., Berkhout, F., Hilderink, H., Hinkel, J., Hof, A., Kitous, A., Kram, T., Mechler, R., and Scrieciu, S.: The use of scenarios as the basis for combined assessment of 960 climate change mitigation and adaptation, Glob. Environ. Chang., 21, 575–591, https://doi.org/10.1016/j.gloenvcha.2010.11.003, 2011.

Wanner, H., Beer, J., Bütikofer, J., Crowley, T. J., Cubasch, U., Flückiger, J., Goosse, H., Grosjean, M., Joos, F., Kaplan, J. O., Küttel, M., Müller, S. A., Prentice, I. C., Solomina, O., Stocker, T. F., Tarasov, P., Wagner, M., and Widmann, M.: Mid- to Late Holocene climate change: an overview, Quat. Sci. Rev., 27, 1791–1828, 965 https://doi.org/10.1016/j.quascirev.2008.06.013, 2008.

Warszawski, L., Frieler, K., Huber, V., Piontek, F., Serdeczny, O., and Schewe, J.: The Inter-Sectoral Impact Model Intercomparison Project (ISI-MIP): project framework., Proc. Natl. Acad. Sci. U. S. A., 111, 3228–32, https://doi.org/10.1073/pnas.1312330110, 2014.

Weiss, H. and Bradley, R. S.: What Drives Societal Collapse?, Science (80-.)., 291, 609–611, 2001.

970 Widmann, M., Goosse, H., van der Schrier, G., Schnur, R., and Barkmeijer, J.: Using data assimilation to study extratropical Northern Hemisphere climate over the last millennium, Clim. Past, 6, 627–644, https://doi.org/10.5194/cp-6-627-2010, 2010.

Williamson, D., Blaker, A. T., Hampton, C., and Salter, J.: Identifying and removing structural biases in climate models with history matching, Clim. Dyn., 45, 1299–1324, https://doi.org/10.1007/s00382-014-2378-z, 2015.

Zhu, Q., Peng, C., Chen, H., Fang, X., Liu, J., Jiang, H., Yang, Y., and Yang, G.: Estimating global natural wetland methane 975 emissions using process modelling: Spatio-temporal patterns and contributions to atmospheric methane fluctuations, Glob. Ecol. Biogeogr., 24, 959–972, https://doi.org/10.1111/geb.12307, 2015.

Zobler, L.: A world soil file grobal climate modeling, NASA Tech. Memo, 32, 1986.